Molecular Cancer Research. 2021 May;19(5):834-846.

Colorectal cancer-derived CAT1-positive extracellular vesicles alter nitric oxide metabolism in endothelial cells and promote angiogenesis.

Atsushi Ikeda[1,2], Satoshi Nagayama[3], Makoto Sumazaki[1,4], Makoto Konishi[1], Risa Fujii[1], Naomi Saichi[1], Satoshi Muraoka[1], Daisuke Saigusa[5], Hideaki Shimada[4], Yoshiharu Sakai[2], Koji Ueda[1*]

[1] Cancer Proteomics Group, Cancer Precision Medicine Center, Japanese Foundation for Cancer Research, Tokyo, Japan.

[2] Department of Surgery, Graduate School of Medicine, Kyoto University, Kyoto, Japan.

[3] Department of Gastroenterological surgery, Cancer Institute Hospital of Japanese Foundation for Cancer Research, Tokyo, Japan.

[4] Department of Surgery, School of Medicine, Toho University, Tokyo, Japan.

[5] Department of Integrative Genomics, Tohoku University Tohoku Medical Megabank Organization, Sendai, Japan.

Corresponding author: Koji Ueda

3-8-31 Ariake, Koto-ku, Tokyo 135-8550, Japan

Tel.: +81 3 3570 0658, Fax.: +81 3 3570 0644, e-mail: koji.ueda@jfcr.or.jp

Competing interests

The authors declare no competing interest about this study.

Running title: CAT1+ EVs Promote Angiogenesis in CRC

Keywords: extracellular vesicles, exosome, colorectal cancer, angiogenesis, CAT1

Molecular Cancer Research. 2021 May;19(5):834-846.

Abstract

Accumulating scientific evidences strongly support the importance of cancer-derived extracellular vesicles (EVs) in organization of tumor microenvironment and metastatic niches, which are also considered as ideal tools for cancer liquid biopsy. To uncover the full scope of proteomic information packaged within EVs secreted directly from human colorectal cancer (CRC), we cultured surgically-resected viable tissues and obtained tissue-exudative extracellular vesicles (Te-EVs). Our quantitative profiling of 6,307 Te-EV proteins and 8,565 tissue proteins from primary CRC and adjacent normal mucosa (n = 17) allowed identification of a specific cargo in CRC-derived Te-EVs, high affinity cationic amino acid transporter 1 (CAT1, $p = 5.0 \times 10^{-3}$, fold change = 6.2), in addition to discovery of a new class of EV markers, VPS family proteins. The EV sandwich ELISA confirmed escalation of the EV-CAT1 level in plasma from CRC patients compared to healthy donors (n = 119, $p = 3.8 \times 10^{-7}$). Further metabolomic analysis revealed that CAT1-overexpressed EVs drastically enhanced vascular endothelial cell growth and tubule formation via upregulation of arginine transport and downstream nitric oxide metabolic pathway. These findings demonstrate the potency of CAT1 as an EV-based biomarker for CRC and its functional significance on tumor angiogenesis.

Implications: This study provides a proteome-wide compositional dataset for viable CRC tissue-derived EVs and especially emphasizes importance of EV-CAT1 as a key regulator of angiogenesis.

Introduction

Colorectal cancer (CRC) is the third most commonly diagnosed cancer and responsible for the second largest number of cancer deaths(1). The five-year survival rate for localized CRC is 89.9%, whereas that for CRC with distant metastasis falls down to 14.2%(2). Therefore, detection of CRC at the earlier stages is essential for effective improvement of the patients' survival. Carcinoembryonic antigen (CEA) is the most widely-used tumor marker for CRC, but it is unsuitable for population screening due to its insufficient sensitivity for early stages of cancer(3). As well as CEA, stool-based tests, including immunochemical or guaiac fecal occult blood tests, are not ideal for screening for CRC because of low sensitivity and specificity(4). On the other hand, colonoscopy is the important screening modality with high sensitivity, but it has a risk of invasiveness accompanying inconvenience for bowel cleansing and unignorable cost(5-9). Moreover, it requires much skill for decent full-bowel examination(10). Thus, development of innovative diagnostics for CRC has been urgently needed, which satisfies both high sensitivity and less invasiveness.

Extracellular vesicles (EVs) are small vesicles released from almost all cell types and play important roles in intercellular communications(11). EVs transport nucleic acids, proteins, metabolites, and other cellular components from donor cells to recipient cells, mediating phenotypic alterations in recipient cells(12-14). Recently, accumulating evidences suggests that EVs can serve as diagnostic modality for a variety of disorders, including malignant diseases(15). We also previously reported a novel strategy to identify EV-based protein biomarkers by comparative proteomic profiling of EVs derived from clear cell renal cell carcinoma(16).

In this study, we isolated EVs from surgically resected viable CRC tissues, which we termed tissue-exudative extracellular vesicles (Te-EVs). We here show

proteomic landscape of Te-EVs derived from primary CRC or adjacent normal mucosa (tumor Te-EVs or normal Te-EVs, respectively), in comparison to quantitative proteome profiles of original tissues. From these datasets, we determined a novel set of EV marker proteins and potential targets for EV-based CRC liquid biopsy. In particular, physiological roles of CAT1 protein on CRC-derived EVs as a meditating factor for angiogenesis in tumor microenvironment are demonstrated.

Methods

Chemicals and antibodies

Monoclonal anti-CD9 (#SHI-EXO-M01), anti-CD63 (#SHI-EXO-M02), and anti-CD81 antibodies (#SHI-EXO-M03) were purchased from Cosmo Bio (Tokyo, Japan). Polyclonal anti-rabbit IgG antibody (Alexa Fluor 488) (#ab150073), polyclonal anti-CAT1 antibody (#ab37588), anti-mouse IgG antibody (20 nm gold preadsorbed) (#ab27242), and anti-rabbit IgG antibody (40 nm gold preadsorbed) (#ab119180) were purchased from Abcam (Cambridge, UK). Polyclonal anti-CAT1 antibody (#14195-1-AP) was purchased from Proteintech (Rosemont, IL). Monoclonal anti-FLAG M2 antibody (#F1804), monoclonal anti-GAPDH antibody (#MAB374), and Polybrene infection reagent (#TR-1003-G) were purchased from Sigma Aldrich (St.Louis, MO). Monoclonal anti-CD31 antibody (#M0823) was purchased from DAKO (Santa Clara, CA). Production of in-house anti-CAT1 polyclonal antibody for EV sandwich ELISA was delegated to Cosmo Bio. In-house polyclonal anti-CAT1 antibody was generated in rabbits immunized with the synthesized peptide comprising amino acid residues 145-160 (CGEFSRTHMTLNAPGVL) of CAT1.

Construction of expression vectors

Total RNA was extracted from HCT116 cells using RNeasy Mini Kit (QIAGEN, Hilden, Germany, #74104) according to the manufacturer's protocol. The cDNA was prepared with Superscript III Reverse Transcriptase (Thermo Fisher scientific, Waltham, MA, #18080044). The ORF sequence of human *SLC7A1* gene, coding CAT1 protein, was amplified with 5'-TTCGCGGCCGCTCGAATGGGGTGCAAAGTCCTGCTCAAC-3' as the forward primer and 5'-AGTCAGCCCGCTCGAGCTTGCACTGGTCCAAGTTGCCG-3' as the reverse primer using the KOD-Plus-Neo kit (TOYOBO, Osaka, Japan, #KOD-401). For transient overexpression experiments, the *SLC7A1* sequence was inserted into the pCAGGS- FLAG vector (pCAGGS-CAT1-FLAG). pCAGGS-FLAG vector was kinfly provided from Dr. Koichi Mtasuda (The Institute of Medical Science, Tokyo University, Tokyo, Japan). For lentiviral stable expression experiments, pCAG-HIVgp (#RDB04394) as a packaging plasmid), pCMV-VSV-G-RSV-Rev (#RDB04393) as an expression vector of VSV-G and Rev proteins), and pCS-CA-MCS (#RDB05963) as a self-inactivating vector plasmid) were provided by RIKEN BRC, Japan. The C-terminal FLAG-tagged CAT1 was inserted into pCS-CA-MCS (pCS-CA-MCS-CAT1-FLAG). Lentiviral vector for CAT1 induction to Human Umbilical Vein Endothelial Cells (HUVEC) were constructed as follows: 293T cells (3.0×10^6) on poly-L-lysine dishes were transfected with pCAG-HIVgp, pCMV-VSV-G-RSV-Rev, and pCS-CA-MCS-CAT1-FLAG or pCS-CA-MCS (as control) using Lipofectamine 3000 (Thermo Fisher Scientific, #L3000001) according to the manufacturer's instruction. After 48 hours incubation, the cultured medium was collected as lentivirus solution (LV-CAT1-FLAG or LV-mock, respectively). For CAT1 induction, HUVEC were infected with LV-CAT1 solution diluted by 50% with the same volume of Endothelial Cell Growth Medium kit with polybrene (10 ng/ml).

Cell culture

Human colon cancer cell line HCT116 was purchased from the American Type Culture Collection, and cultured in RPMI1640 (FUJIFILM Wako Pure Chemical Corporation, Osaka, Japan) with 10% fetal bovine serum (Thermo Fisher scientific). Human Embryonic Kidney cell line 293T was purchased from the American Type Culture Collection, and cultured in DMEM (FUJIFILM Wako Pure Chemical Corporation) with 10% fetal bovine serum. HUVEC were purchased from PromoCell (Heidelberg, Germany, #C12203), and cultured in Endothelial Cell Growth Medium kit (PromoCell, #C22110). All cell lines were cultured with 1% penicillin/streptomycin mixture (FUJIFILM Wako Pure Chemical Corporation).

Clinical samples

All clinical samples were obtained at Cancer Institute Hospital of Japanese Foundation for Cancer Research, Tokyo, Japan. The clinicopathological information of the patients and healthy donors is summarized in Supplementary Table 1. Cancer staging was done according to the seventh edition of the TNM Classification of Malignant Tumors from Union for International Cancer Control. Written informed consents were obtained from all study participants. The procedures involving human subjects are in agreement with the Declaration of Helsinki. This research was approved by the institutional ethics review board.

Isolation of extracellular vesicles

Tissues of primary CRC and adjacent normal mucosa were freshly obtained from CRC patients undergoing colorectal resection in our hospital. Isolation and purification of Te-EVs were performed as follows. The 3-5 mm cubes of the excised tissues were rinsed with PBS and incubated in 1.5 ml of RPMI1640 with gentle rotation at 37°C for 3 hours. The culture medium was centrifuged at 3,000

× *g* for 5 min and then 12,000 × *g* for 30 min to remove larger debris. Te-EVs were isolated with centrifugation of 100,000 × *g* for 1 h, and purified by two cycles of washing with 1 ml of PBS and centrifugation at 100,000 × *g* for 1 h as a pellet. To generate CAT1-overexpressing EVs ($CAT1^{++}$-EVs), HCT116 cells were transfected with pCAGGS-FLAG-CAT1 vector using Lipofectamine 3000 according to manufacturer's instructions, followed by replacement of medium to RPMI1640 with the Exosome-depleted FBS (Thermo Fisher Scientific, #A2720801) 24 hours after the transfection. For a control, mock-EVs were also prepared from the supernatant of the empty pCAGGS vector-transfected HCT116 cells. Following 48 hours incubation, the culture medium was collected and centrifuged at 2,000 × *g* for 5 min and then 10,000 × *g* for 30 min to remove larger debris. Ultracentrifugal purification of EVs was performed with the same manner as Te-EVs above. Protein concentrations of EV lysates were measured using Micro BCA Protein Assay Kit (Thermo Fisher Scientific, #23235)

Protein extraction from tissues

Proteins were extracted from the original tissues (primary CRC or adjacent normal mucosa). Approximately 3 mm^3 of the tissue was homogenized in 400 µl of Phase Transfer Surfactant (PTS) buffer [20 mM HEPES-NaOH (pH 7.6), 12 mM sodium deoxycholate, 12 mM sodium *N*-Lauroylsarcosinate] using a probe sonicator. After centrifugation at 15,000 × *g* for 15 min, the supernatant was quantified with Micro BCA Protein Assay Kit.

Liquid chromatography mass spectrometry (LC/ MS) analysis

Protein samples (10 µg) were dissolved in Laemmli's SDS sample buffer, reduced with 20 mM TCEP at 37°C for 30 min, and then alkylated with 50 mM iodoacetamide at ambient temperature in a dark for 45 min. These samples were

subjected to 10% polyacrylamide gel electrophoresis. The electrophoresis was stopped at the migration distance of 2 mm from the top edge of the separation gel. After CBB-staining, protein bands were excised, destained, and cut finely prior to in-gel digestion with Trypsin/Lys-C Mix (Promega, #V5073) at 37°C for 12 hours. The resulting peptides were extracted from gel fragments and analyzed by Orbitrap Fusion Lumos mass spectrometer (Thermo Scientific) combined with UltiMate 3000 RSLC nano-flow HPLC (Thermo Scientific) equipped with 0.075 × 150 mm C_{18} tip-columns (Nikkyo Technos, Tokyo, Japan). A two-step linear gradient comprising 2-35% acetonitrile for 95 min and 35-95% acetonitrile for 15 min in 0.1% formic acid at flow rate of 250 nL/min was utilized. The eluates were directly ionized with a spray voltage of 2 kV. Spectra were collected by Full MS ion scan mode over the m/z range 350-1500 with 60,000 resolution. CID MS/MS scans were acquired with the Ion trap detector up to 2 seconds for each MS full scan event under data-dependent acquisition mode with the dynamic exclusion function enabled. The raw data are available at a public proteomic database, Japan Proteome Standard Repository/Database (jPOST), ID: JPST000867(17).

Identification and label-free quantification of proteins

Protein identification and label-free quantification were performed on the Proteome Discoverer 2.2 software (Thermo Fisher Scientific). For protein identification, the LC/MS dataset was searched against SwissProt Human Database with Mascot (Matrix Science, London, UK) or Sequest HT (Thermo Fisher Scientific) database search engine, where false discovery rate < 1% was set for peptide identification threshold. For label-free quantification and data normalization, the Minora Feature Detector node in the Processing workflow and the Feature Mapper node followed by the Precursor Ions Quantifier node in the

Consensus workflow were employed with default parameters in the Proteome Discoverer 2.2 software.

Statistical analysis

Proteomic compositions were compared between tumor Te-EVs and normal Te-EVs using paired t-test. Then the *p*-Values were adjusted to control false discovery date less than 5%, using Benjamini-Hochberg Procedure (18). Proteins satisfying the criteria (adjusted $p < 0.05$, fold-change > 5.0, and valid value > 50%) were defined as statistically differential protein cargoes. Box plots, a violin plot, and ROC curves were depicted by R 4.0.0. Principal component analysis was performed by the Analyst module in Expressionist server platform (Genedata AG, Swiss). Continuous variables were analyzed using Student's t test, and categorical valuables with Pearson's χ^2 test or Fisher's exact test, as appropriate. Statistical analysis was performed using JMP software version 13.0 (SAS Institute, Cary, NC). $p < 0.05$ was considered statistically significant.

Western blotting analysis

Cells were lysed with RIPA buffer [50 mM Tris-HCl (pH 7.8), 150 mM NaCl, 1% Triton X-100, 0.1% SDS, 0.5% sodium deoxycholate, and 1 mM EDTA] containing Complete protease inhibitor cocktail (Roche Diagnostics, Mannheim, Germany, #11873580001). Proteins were separated on 8-12.5% SDS polyacrylamide gels and transferred onto PVDF membranes (Merck-Millipore, #IPVH00010). Following blocking with 4% Block Ace (Yukijirushi Nyugyo, Tokyo, Japan, #UK-B80), membranes were incubated with the first antibodies. Membranes were then incubated with HRP–conjugated anti-mouse IgG (GE Healthcare, Chicago, IL, #NA931-1ML) or anti-rabbit IgG (GE Healthcare, #NA934-1ML) and detected with Western Lightning ECL Pro (Perkin Elmer, MA,

#NEL121001EA). Quantification of band intensity was performed using Image Lab software version 5.2 (Bio-Rad Laboratories, Hercules, CA).

Immunohistochemical (IHC) analysis

A total of 80 sets (20 sets for every stage) of CRC tissue and adjacent normal mucosa was sectioned in 5 μm thick by the microtome system. The deparaffinization, rehydration, and IHC were automatically carried out on the Leica Bond III Automated IHC and ISH system (Leica Microsystems Ltd) with polyclonal anti-CAT1 antibody (Proteintech) and anti-CD31 antibody. The expression levels of CAT1 were classified into 3 categories; 0: no expression, 1: slightly expressed, and 2: moderately to strongly expressed. Using the categorized data, the expression levels of CAT1 of CRC tissue were compared with those of adjacent normal tissues.

To evaluate the expression of CAT1 in vascular endothelial cells of the CRC tissues and adjacent normal tissues, 70 pairs of slides were investigated. The rates of moderate to strong-CAT1 expression in vascular endothelial cells were compared between in or near CRC tissues and adjacent normal tissues.

Transmission electron microscope (TEM) analysis

TEM analysis was performed as previously reported(19). Briefly, EV samples (10 μg) were fixed with 2% paraformaldehyde and incubated with polyclonal anti-CAT1 antibody. Immunoreactive EVs were visualized with the second antibody preadsorbed with the 20 nm gold (anti-mouse IgG antibody, Abcam, #ab2724) for Te-EVs or 40 nm gold (anti-rabbit IgG antibody, Abcam, #ab119180) for $CAT1^{++}$-EVs and mock-EVs, and observed with H-7650 (HITACHI, Tokyo, Japan).

EV sandwich ELISA

After immobilization of the in-house anti-CAT1 antibody (250 ng) on the bottom of Nunc-immuno plate II (Thermo Fisher Scientific, #442404), surface of wells was blocked with 5% BSA in PBS for 30 min. Following 3 hours incubation of plasma samples (10 µl) with PBS (90 µl), wells were washed with PBS 3 times and incubated with 100 ng of biotinylated anti-CD81 antibody in 1% BSA for 1 hour. After 3 times wash steps, 100 µl of 30,000-fold diluted Streptavidin poly-HRP40 (Stereospecific Detection Technologies, #SP40D50) was added and incubated for 45 min, followed by PBS washing. HRP activity was detected with 1-Step Ultra TMB-ELISA Substrate Solution (Thermo Fisher Scientific, #34028). The absorbance at 450 nm was read by Sunrise microplate reader (Tecan, Männedorf, Switzerland). All procedures were done at room temperature. To normalize the absorbance data among the plates, we prepared standard curves by plotting different concentrations of purified CAT1^{++}-EVs. In each plate, we defined the absorbance signal produced by 1.0 µg of CAT1^{++}-EVs as 1 unit. To construct a combination diagnostic model using EV-CAT1 and CEA, logistic regression model was employed for maximization of area under the curve of the receiver operating characteristics (ROC) curve; $log(p/1-p) = 1.45 - 14.1x_1 - 0.56x_2$ (x_1: EV-CAT1 concentration, x_2: CEA concentration).

EV incorporation assay

To monitor a short-term EV incorporation, HUVEC (3.0×10^4 cells / well) were seeded on 8-well chamber slides (0.7 cm^2/well, Thermo Scientific) and cultured for 12 h. PKH26GL-labeled (Sigma-Aldrich, #PKH26GL) CAT1^{++}-EV (6 µg) or PBS (as control) were added and incubated for 4 hours. Following 3 times washes by PBS, the cells were fixed with 4% paraformaldehyde. The slides were

mounted with VECTASHIELD Mounting Medium with DAPI (Vector Laboratories, Burlingame, CA, #H1500) and observed with fluorescent microscope (IX83, Olympus, Tokyo, Japan). To confirm a long-term EV-mediated transfer of CAT1 protein, HUVEC (5.0×10^4 cells / well) were seeded on 24-well plates and cultured for 12 hours. CAT1^{++}-EVs (5 μg) or PBS (as control) were then added and incubated for further 12, 24, or 36 hours. After blocking with 1% BSA and fixing with 4% paraformaldehyde, cells were incubated with polyclonal anti-CAT1 antibody (Abcam) for an hour, followed by subsequent staining with anti-rabbit IgG antibody (Alexa Fluor 488) for an hour. Finally, the slides were mounted with VECTASHIELD Mounting Medium with DAPI and observed with fluorescent microscope IX83.

Cell growth assay

HUVEC (2×10^3 cells / well) were seeded on 96-well plates and cultured for 24 hours. CAT1^{++}-EV (1 μg), mock-EV (1 μg), or PBS (as control) were added and incubated for further 24, 48, or 72 hours. After incubation, cells were treated with Cell Counting Kit-8 reagent (Dojindo, Kumamoto, Japan, #CK04) for 2 hours and the absorbance at 450 nm of the culture medium was read with Sunrise microplate reader.

Tube formation assay

HUVEC (8×10^4 cells / well) mixed with CAT1^{++}-EV (10 μg) or mock-EV (10 μg) were seeded on Geltrex Matrix-coated 24-well plates (Thermo Fisher Scientific, #A1569601) and cultured for 16 hours. HUVEC cultured in the matrix form structures that mimic a pseudo capillary pattern, leading to meshed tube networks. The cells were stained with 2 μg/ml of Calcein AM (Thermo Fisher Scientific, #C1430) at 37 °C for 30 min and observed with fluorescent microscope

IX83. Images were obtained at four non-overlapping, randomly selected fields at each well. The total length of the tube network was extracted from the images using NIH Image J software (ver. 1.52i) and Angiogenesis Analyzer plugin (20), available at the website: http://image.bio.methods.free.fr/ImageJ/?Angiogenesis-Analyzer-for-ImageJ&lang=en.

Metabolome analysis

HUVEC were transfected with LV-CAT1 or LV-mock (HUVEC-CAT1 or HUVEC-mock, respectively) and polybrene (10 μg/ml, final concentration). After serum starvation for 12 hours, HUVEC-CAT1 or HUVEC-mock cells (5×10^7) were stimulated with the Endothelial Cell Growth Medium for 15 min. Cells were rinsed with ice-cold PBS twice and immediately scraped off from dishes. For analyses of arginine, Citrulline, NG-Hydroxy-L-arginine (NHA), guanosine triphosphate (GTP), nicotinamide adenine dinucleotide phosphate (NADPH), and nicotinamide adenine dinucleotide phosphate (NADP), 200 μl of methanol including $^{13}C_6$-Arginine (1 μg/ml) as an internal standard (IS) was added and stirred in an ultrasonic bath. Samples were centrifuged at 16,400 × *g*, 4°C for 10 min, and 130 μl of the supernatants were concentrated to 40 μl by centrifugal evaporator. Finally, 3 μl of the concentrated sample was subjected to LC-MS/MS analysis. Analytical methods for multiple reaction monitoring (MRM) were described previously(21). Analysis of cyclic guanosine monophosphate (cGMP) was performed as reported previously with several modification(22,23). The cell pellet was re-suspended in 100 μl homogenization buffer containing 10 mM Tris-HCl (pH 7.4), 10% glycerol, and 10 μM cytosine-2,4-$^{13}C_2$,$^{15}N_3$ as an IS. After homogenization, proteins were removed by adding 350 μl of acetonitrile, followed by centrifugation at 16,400 × *g*, 4°C for 15 min. Subsequently, 405 μl of the supernatant was vacuum-dried and dissolved in 90 μl of 0.1% (v/v) formic acid in

water. The injection volume was 10 µl. The metabolites were measured using the LC/MS system (TSQ Quantiva, Thermo Scientific) equipped with NANOSPACE SI-2 (OSAKA SODA, Osaka, Japan). Chromatographic separation was performed using ZIC-pHILIC column (2.1 × 100 mm, Sequant, Darmstadt, Germany) for arginine, citrulline, GTP, NADPH, NHA, and NADP analyses or Discovery HS F5 column (2.1 × 150 mm, Sigma-Aldrich) for cGMP analysis. Data acquisition and analysis were done by Xcalibur software (Thermo Scientific). All analyses were done in triplicate.

cGMP ELISA

HUVEC (1×10^7) were incubated with 80 µg of CAT1^{++}-EVs or mock-EVs for 24 hours. After serum starvation for 12 hours, HUVEC were stimulated with the Endothelial Cell Growth Medium for 15 min. Collected cells were lysed, and subjected to cGMP ELISA. The assay was performed using cGMP ELISA Kit (Cayman Chemical, Ann Arbor, MI, #581021) according to the manufacturer's instruction with acetylating protocols.

Results

Isolation of extracellular vesicles from viable resected tissues

Fig. 1a shows a schematic overview illustrating isolation of tissue-exudative extracellular vesicles (Te-EVs) from surgically resected CRC or adjacent normal mucosa (n = 17). Three hours incubation of tissues with gentle rotation secreted a sufficient amount of Te-EVs (98.7 ± 76.7 µg total EV proteins). When the efficiency of EV enrichment was assessed with western blotting analyses, expression levels of typical EV marker proteins, CD63 and CD81, were significantly higher in Te-EV samples than those in total tissue lysates (Fig. 1b, c). These molecular features and results of subsequent proteome profiles (Fig.

2b, c, d) indicated that EVs were efficiently released and collected from viable CRC tissues as Te-EVs.

Comprehensive proteome analysis of Te-EVs and original tissues

From LC/MS analyses, 8,565 tissue proteins and 6,307 Te-EV proteins (Supplementary Table 2 and 3, respectively) were identified with peptide FDR < 1% (9,854 non-redundant proteins in total). Among them, 5,018 proteins were commonly identified in both tissues and Te-EVs (Fig. 2a), for which, interestingly, only limited quantitative relationship was observed (R^2 = 0.185, Fig. 2b). This fact represented a large compositional difference between EV proteome and the original cell proteome, suggesting that highly selective loading of protein cargoes may occur during construction of EVs. Indeed, as reported previously, tetraspanin family proteins were significantly enriched in EVs compared to intracellular levels (Fig. 2c). Notably, we found for the first time that vacuolar protein sorting (VPS) family proteins were more characteristically loaded in EVs (Fig. 2d), which would be useful as specific EV luminal protein markers. As for the identified 6,307 total Te-EV proteins, 3,620 proteins (57.3%) were already cataloged in the most common EV database, ExoCarta, whereas we further added 2,687 new entries as EV cargo proteins (Fig. 2e). When focused on colorectal cancer cell-derived EVs, 6,166 proteins were found in Te-EVs from tumor regions of CRC tissues (tumor Te-EVs), in which 4,877 proteins (79.1%) were newly identified in this study (Fig. 2f). Thus, in addition to thoroughly optimized proteomic analysis by the high-end LC/MS system, our strategy for isolation of the high-purity EVs in serum-free media allowed such in-depth analysis of EV proteins (> 10^8 of dynamic range, Supplementary Fig. 1), including discovery of a new class of EV marker proteins, the VPS family. Indeed, to our knowledge, the dataset to 6,307

protein identification is the largest one ever as a report of single set of EV proteomics analysis.

Specific protein cargoes on colorectal cancer cell-derived EVs

To clarify specific molecular signatures in viable CRC tissue-derived EVs, which should serve as ideal targets of CRC diagnosis or therapy, paired t-test was employed for comparison of proteome in normal Te-EVs with that in tumor Te-EVs, then the *p*-Values were adjusted to control false discovery rate less than 5%. As the result, 487 proteins (Supplementary Table 4) were found to be significantly enriched in tumor Te-EVs (adjusted $p < 0.05$ and fold-change > 5.0), while 88 proteins were diminished (adjusted $p < 0.05$ and fold-change < 0.2) (Fig. 3a). Principle component analysis confirmed that top 100 of the up-regulated proteins in tumor Te-EVs were sufficient to classify 17 pairs of samples into two groups, normal mucosa tissue-derived EVs or colorectal cancer tissue-derived EVs (Fig. 3b). Interestingly, gene ontology (GO) analysis of the 487 proteins revealed that regulators of gene expression were highly loaded into tumor Te-EVs, whereas response elements against external stimulations were purged from them (Supplementary Fig. 2). Such characteristic selection of protein cargoes may define the modes of functional manipulation of the CRC microenvironment by EVs.

For the purpose of establishing a novel tool for CRC liquid biopsy based on the dataset above, we further focused on 11 cell surface proteins out of 487 cargoes specifically-loaded in tumor Te-EVs (Supplementary Table 5), for which direct detection with “EV sandwich ELISA” (Fig. 4a) is applicable. The extraction of the cell surface proteins was done by selecting proteins which were annotated to contain a transmembrane domain, available at the Uniprot database. Particularly, solute carrier family 7 member 1 / high affinity cationic amino acid transporter 1

(SLC7A1/CAT1) was estimated to be a solid candidate of a CRC biomarker due to its overexpression in CRC tissues(24). As the result of our LC/MS-based label-free quantification, the expression levels of CAT1 were significantly higher on tumor Te-EVs compared to those on normal Te-EVs ($p = 5.0 \times 10^{-3}$, fold change = 6.2, Fig. 3c). The expression of CAT1 on the surface of tumor Te-EVs was ensured by the gold-labeled anti-CAT1 antibody and transmission electron microscope (TEM) in Fig. 3d. The expression of CAT1 was observed in 32.4% of tumor Te-EVs, while none of normal Te-EVs expressed CAT1 on their surfaces. The result of LC/MS analysis was confirmed by western blotting analysis using Te-EVs from the independent sample set (n = 10, Fig. 3e), showing significantly higher expression of CAT1 on tumor Te-EVs ($p = 0.01$, Fig. 3f).

To figure out the origin of CAT1^{++}-EVs, we next evaluated CAT1 expression levels in tissue samples by immunohistochemical staining analysis of the CRC tissue array slide (n = 75). As shown in the representative images (Fig. 3g) significantly higher expression of CAT1 was observed in CRC cells, while none or weak expression was only detected in normal colon mucosa ($p = 6.4 \times 10^{-8}$), although stage-dependent tendency was not observed (Fig. 3h). This result could support an idea that the CAT1-overexpressed EVs (CAT1^{++}-EVs) might be biogenerated and released from CRC cells.

A diagnostic potential of plasma EV-CAT1 for detection of CRC

To evaluate a diagnostic power of EV-CAT1 as a peripheral blood biomarker for CRC, we constructed a high throughput EV sandwich ELISA (Fig. 4a) which allowed simultaneous quantification of CAT1 abundances on EVs from 96 crude plasma samples. The result of EV-CAT1 measurement from 119 cases (25 health donors, 23 CRC stage I patients, 25 stage II patients, 25 stage III patients, and 21 stage IV patients) was displayed as a box plot in Fig. 4b. Statistical

assessments revealed that the concentrations of EV-CAT1 in CRC patients' plasma (0.22 ± 0.24 unit) were significantly elevated compared to those in healthy donors' plasma (0.082 ± 0.10 unit/ml) ($p = 3.8 \times 10^{-7}$). Importantly, the escalation of EV-CAT1 level was observed even in the stage-I group (0.19 ± 0.17 unit) ($p = 1.8 \times 10^{-6}$), indicating high potency for detection of CRC. In comparison with the existing biomarker CEA in the same cohort (n = 119) (Supplementary Table 1) by ROC curve analysis, the detection efficacy of EV-CAT1 was slightly better (AUC = 0.821, 95% CI: 0.732 - 0.909) than CEA (AUC = 0.780, 95% CI: 0.690 - 0.870) (Fig. 4c). But, due to independent tendency of positivity (Supplementary Fig. 3), a combination diagnostic model using EV-CAT1 and CEA demonstrated much better detection efficiency (66.7% sensitivity, 92.0% specificity, and AUC = 0.907, 95% CI: 0.850 - 0.963). These data could encourage us to conduct further efforts about EV-CAT1 using a larger cohort for more solid confirmation as a clinically-applicable biomarker in the future study.

EV-mediated transfer of CAT1 promotes growth of vascular endothelial cells and enhances tubule formation in CRC microenvironments

According to the datasets above, it was a fact that CAT1 protein was overexpressed on both CRC cells and CRC-derived EVs. However, a physiological relevance of CAT1 overexpression on EVs to CRC development was still unclear. Therefore, in order to explore preferential recipient cells of $CAT1^{++}$-EVs, CAT1-upregulated cells (except for cancer cells) were searched in the microenvironments of CRC tissues using immunohistochemical staining analysis (Fig. 5a). From this observation, interestingly vascular endothelial cells near or inside CRC tissues showed significantly stronger signals of CAT1 than those in adjacent normal tissues (Fig. 5b). Considering high expression of CAT1

on tumor Te-EVs, we speculated that CRC cells might transfer CAT1 protein to vascular endothelial cells via EVs.

To clarify this functionally, we at first prepared CAT1^{++}-EVs from CAT1-overexpressed HCT116 cells, for which specific expression of CAT1 was confirmed by western blotting analysis (Fig. 5c). Moreover, transmission electron microscopy (TEM) images depicted the CAT1 expression on surface of EV membrane (Fig. 5d). Then we treated vascular endothelial cell HUVEC with CAT1^{++}-EVs and investigated their behavior and influence on HUVEC *in vitro*. After 4 hours exposure of fluorescence-labeled CAT1^{++}-EVs to HUVEC, lots of sporadic fluorescent signals were observed in the cells (Fig. 5e), showing that CAT1^{++}-EVs were incorporated into intracellular region of HUVEC. From an elongated period of observation (after 3 days), we found a dotted pattern of CAT1 expression on the surface of cells (Fig. 5f). This image clearly demonstrated that an amino acid transporter protein CAT1 was finally reconstituted to its innate subcellular location after EV-mediated transportation. The transportation of CAT1 via EV was supported by higher expression of CAT1 observed in CAT1^{++}-EV-treated HUVEC compared with those treated with mock-EV (Fig. 5g).

Importantly, the CAT1^{++}-EV-treated HUVEC, which showed ectopic CAT1 expression (Fig. 5h), exhibited significantly upregulated growth speed compared to those treated with mock EVs (n = 3, p = 0.026) (Fig. 5i) Western blotting analysis of HUVEC used in the cell growth assay showed high expression of CAT1 in HUVEC treated with CAT1^{++}-EV compared with HUVEC treated with PBS or mock-EV. When the CAT1^{++}-EV-treated HUVEC were placed in thin 3D matrigel culture plates, these cells also showed faster formation of tubular structures (Fig. 5j, k) (p = 0.01). These data suggested that EV-mediated excessive supply of CAT1 to vascular endothelial cells might promote angiogenesis in CRC microenvironment.

Overexpressed CAT1 promotes angiogenesis by modulating cGMP metabolism

Considering CAT1's well-known function of transporting extracellular arginine, which is a substrate for the synthesis of key angiogenic modulator nitric oxide (NO) in the vascular endothelium (25,26), we focused on NO-signaling pathways to clarify the molecular mechanism of pro-angiogenic effect exerted by $CAT1^{++}$-EVs. For the list of 487 tumor Te-EV up-regulated protein cargoes (Supplementary Table 4), GO-based functional profiling revealed that proteins associated with regulation of nitrogen compound metabolic process (GO:0051171) and organonitrogen compound biosynthetic process (GO:1901566) were significantly enriched (Supplementary Table 7a). For instance, key regulators of the NO synthesis pathway, such as NAD(P)H dehydrogenase [quinone] 1 (NQO1) (fold change = 19.5) (27), Dihydrofolate reductase (fold change = 5.9) (28), FAD synthase (fold change = 6.3) (29), and Sepiapterin reductase (SPR) (fold change = 5.7) (30) were linked to these GO terms, indicating that NO production in the EV-targeted cells would be promoted concurrently with CAT1 (31). To confirm NO signaling pathway initiated by CAT1 in vascular endothelial cells, MRM-based targeted metabolome analysis was performed using CAT1-overexpressed HUVEC (HUVEC-CAT1) or mock vector-transfected HUVEC (HUVEC-mock) (Fig, 6a). Absolute quantification measurements for NO-related metabolic pathways revealed that arginine, nicotinamide adenine dinucleotide phosphate (NADP), and cGMP were significantly up-regulated in HUVEC-CAT1 after serum stimulation (Fig. 6b). On the contrary, GTP was down-regulated in HUVEC-CAT1 compared with HUVEC-mock. Direct measurement of cGMP in HUVEC treated with $CAT1^{++}$-EVs revealed significantly higher concentration than in HUVEC treated with mock-EVs,

which confirms the metabolomic alteration via EVs in physiologic context (Fig. 6c). Considering that cGMP activates cGMP-dependent protein kinase (PKG) which was reported to promote angiogenesis through activation of both ERK and p38 signaling pathways (32), it is suggested that overexpressed CAT1 in HUVEC, brought by $CAT1^{++}$-EV, may contribute to angiogenesis in the microenvironments of CRC (Fig. 6d).

DISCUSSION

In this study, 6,307 protein components of EVs were cataloged, which directly derived from resected fresh tissues of CRC patients (Te-EVs). In fact, both the comprehensiveness of protein IDs and the quantitative depth of this EV proteome analysis ($> 10^6$) are maximum at present (Supplemental Fig. 3). It is notable that the number 6,307 protein IDs exceeded the ExoCarta repository (5,875 proteins) composed of previously published EV proteome datasets (33) . For in-depth omics analysis of EVs, thorough purification of EVs, as well as optimal analytical technologies, are indispensable. From this point of view, the unique characteristics of Te-EVs fits the requirement well. Since the viable tissue blocks are cultured in serum-free medium for a short term, only minimal amount of free proteins (such as albumin, IgG, IgA, transferrin, and so on) are included, meaning that excessive purification procedures are not needed for obtaining high-purity EVs. More importantly, in contrast to blood- or urine-derived EV samples, Te-EVs do not contain whole body-derived EVs, allowing specific molecular profiling of disease site-derived EVs. It is also critically important that a pair of tumor- and normal tissue-derived EVs with an identical genetic background is available individually. This fact facilitates precise identification of cancer specific cargoes in tumor tissue-derived EVs regardless of noises of individual variations. Additionally, Te-EVs are amplifiable by elongated culture duration, suggesting

that a wide range of EV analyses would be practicable even from tiny biopsy samples or precious clinical specimens. Indeed, all the advantages above lead our first challenge about the study of Te-EVs from clear cell renal cell carcinoma (ccRCC) to successful identification of a potential diagnostic biomarker on EV (EV-AZU1) which showed specific load on the surface of ccRCC-derived EVs ($n = 20$, $p = 2.85 \times 10^{-3}$, fold-change = 31.6)(16). Furthermore, an EV-mediated key regulator of Akt signaling in ccRCC, EV-LAIR1, was also found, which would possess a great potential as a target of ccRCC therapy(34). Thus, including the present study about CRC, application of Te-EV could accelerate biological elucidation of molecular characteristics of physiologically secreted EVs from any solid tumors and also clinical development of EV biomarkers and therapeutics.

In addition to 6,307 EV proteins, here we acquired quantitative profiles of 8,565 proteins in original tissues (in total 9,854 non-redundant proteins). Quantitative and qualitative comparison between EV proteome and original tissue proteome could help to settle the important question of whether a subset of protein cargoes would be actively transported into EVs or passively distributed to EVs (Supplementary Fig. 4, Supplementary Table 6). The proteomic distribution of subcellular location in Te-EVs are similar with that in original tissues (Supplementary Fig. 5). Considering that the quantitative expressions of Te-EV proteome is not relative to that of original tissue proteome (Fig. 2c), there should be a mechanism of active transportation of certain proteins into EVs regardless of their subcellular locations. In addition to identification of a new class of EV luminal markers, VPS family (Fig. 2d), this knowledgebase would make a large contribution to unravel the biogenesis of EVs and the biological significance of their existence.

In the present study, we showed involvement of CAT1 in activation of the NO metabolic cascade. Considering the function of NO as a direct effector for tumor angiogenesis(25,26), tumor Te-EVs may play a role to promote angiogenesis in the tumor microenvironments. CRC cells might secrete “customized” EVs for transferring such proteins to mediate the phenotype of EV-targeted cells, leading to microenvironment alteration favorable for their survival, development, or metastasis. On the other hand, KEGG pathway analysis for 487 proteins above demonstrated enrichment of pathways related to viral infections (Supplementary Table 7c). Previous study reported high prevalence of CRC in virus-infected patients, including human papilloma virus and Epstein-Barr virus(35). This fact may reflect the passive transport of proteins related to viral infections, transforming the environment into favorable one for CRC expansion.

Recently, EVs have been attracting a fair amount of interest from increasing researchers as a promising tool for diagnostic and prognostic biomarkers(36,37). In this study, the plasma EV-CAT1 measurement demonstrated a good potential to be used for detection of earlier stages of CRC cases (Fig. 4b). Indeed, EV-CAT1 complemented the sensitivity of CEA at the earlier stages of CRC, resulting in reinforcement of diagnostic power in the combination model of EV-CAT1 and CEA, compared to the single use of CEA (Fig. 4c). Importantly, the experimental procedures of the EV sandwich ELISA are identical with those of the traditional sandwich ELISA, which can be smoothly automated with a similar cost of general tumor markers. Given these features and the fact that the detection property of EV-CAT1 was independent of CEA (Supplementary Fig. 3), a complementary use of EV-CAT1 measurement with CEA in a cancer screening would enhance an opportunity of detecting CRC by a non-invasive blood test, although larger-scaled preclinical validation study should be necessary.

CAT1 is one of the cationic amino acid transporter family proteins and considered as the most major carrier of arginine, lysine, and ornithine(38-40). CAT1 transfers extracellular arginine directly to the membrane-bound endothelial NO synthase (eNOS) which is co-localized with CAT1 in a caveolae(41), leading to production of NO. NO is reported to initiate various intracellular signaling pathways including activation of soluble guanylate cyclase (sGC) which converts GTP to cGMP(42). Then cGMP binds to four sites on the regulatory subunits of cGMP-dependent protein kinase (PKG), inducing activation of the catalytic subunit of PKG. In the present study, we visually showed EV-mediated transfer of CAT1 from CRC cells to the surface of vascular endothelial cells (Fig. 5e) and accumulation of arginine, NADP, and cGMP in CAT1-overexpressed cells after growth stimulation (Fig. 6b). Moreover, cGMP up-regulation in vascular endothelial cells mediated by CAT1-overexpressed EVs were observed, which confirmed the impact of CAT1 on EVs in more physiologic context. All of these known metabolic pathways and our data suggested that intact CRC cells might manipulate the cGMP-dependent signals in surrounding vascular endothelial cells. Indeed, PKG is known to strongly activate both ERK and p38 MAPK signaling pathways. Previous studies showed that PKG promotes proliferation of vascular endothelial cells by phosphorylating Raf-1 and activation of the Raf-MEK-ERK signal transduction(32). On the other hand, p38 activates MAP kinase-activated protein kinase 5 (MAPKAPK5) by phosphorylation of Thr-182, which mediates migration of vascular endothelial cells toward tumors and incorporation of them into a tumor vasculature through activation of Focal adhesion kinase 1 (FAK)(43). In consideration of our data that extrinsic CAT1 significantly promoted tube formation of vascular endothelial cells in matrigel (Fig 5h and 5i), CRC-derived $CAT1^{++}$-EVs may act as an attractant of angiogenic blood vessels by activating the arginine-NO-cGMP metabolic pathway and ERK/p38

phosphorylation signals in vascular endothelial cells. In the biology of CRC, Vascular endothelial growth factor (VEGF) is a well-established key regulator of angiogenesis, which induces both ERK and p38 signals(44), indicating that CAT1^{++}-EVs and VEGF would coordinately activate different angiogenic pathways around the microenvironment of CRC.

In conclusion, encyclopedic database about 6,307 Te-EV proteins and 8,565 original tissue proteins were filed for CRC based on in-depth proteomic analysis, where a novel EV-based biomarker CAT1 was found. Our strategy to utilize Te-EVs can be applied to other modalities of analyses, such as DNA, miRNAs, metabolites, and so on, for any solid tumors or non-cancer diseases. CAT1^{++}-EVs promoted cell growth of vascular endothelial cells via arginine-oriented metabolic and phosphorylation pathways, implicating that they could also serve as novel druggable pathways in CRC in the future.

REFFERENCES

1. Bray F, Ferlay J, Soerjomataram I, Siegel RL, Torre LA, Jemal A. Global cancer statistics 2018: GLOBOCAN estimates of incidence and mortality worldwide for 36 cancers in 185 countries. CA: a cancer journal for clinicians **2018**;68(6):394-424 doi 10.3322/caac.21492.
2. SEER Cancer Statistics Review. <https://seer.cancer.gov/statfacts/html/colorect.html>.
3. Fletcher RH. Carcinoembryonic antigen. Ann Intern Med **1986**;104(1):66-73 doi 10.7326/0003-4819-104-1-66.
4. Ahlquist DA, Wieand HS, Moertel CG, McGill DB, Loprinzi CL, O'Connell MJ*, et al.* Accuracy of fecal occult blood screening for colorectal neoplasia. A prospective study using Hemoccult and HemoQuant tests. JAMA **1993**;269(10):1262-7.
5. Gatto NM, Frucht H, Sundararajan V, Jacobson JS, Grann VR, Neugut AI. Risk of perforation after colonoscopy and sigmoidoscopy: a population-based study. J Natl Cancer Inst **2003**;95(3):230-6 doi 10.1093/jnci/95.3.230.
6. Segnan N, Senore C, Andreoni B, Azzoni A, Bisanti L, Cardelli A*, et al.* Comparing attendance and detection rate of colonoscopy with sigmoidoscopy and FIT for colorectal cancer screening. Gastroenterology **2007**;132(7):2304-12 doi 10.1053/j.gastro.2007.03.030.
7. Lansdorp-Vogelaar I, Goede SL, Bosch LJW, Melotte V, Carvalho B, van Engeland M*, et al.* Cost-effectiveness of High-performance Biomarker Tests vs Fecal Immunochemical Test for Noninvasive Colorectal Cancer Screening. Clin Gastroenterol Hepatol **2018**;16(4):504-12 e11 doi 10.1016/j.cgh.2017.07.011.
8. Nicholson FB, Korman MG. Acceptance of flexible sigmoidoscopy and colonoscopy for screening and surveillance in colorectal cancer prevention. J Med Screen **2005**;12(2):89-95 doi 10.1258/0969141053908294.
9. Levin B, Lieberman DA, McFarland B, Smith RA, Brooks D, Andrews KS*, et al.* Screening and surveillance for the early detection of colorectal cancer and adenomatous polyps, 2008: a joint guideline from the American Cancer Society, the US Multi-Society Task Force on Colorectal Cancer, and the American College of Radiology. CA Cancer J Clin **2008**;58(3):130-60 doi 10.3322/CA.2007.0018.
10. Rodrigues-Pinto E, Ferreira-Silva J, Macedo G, Rex DK. (Technically) Difficult colonoscope insertion - Tips and tricks. Dig Endosc **2019** doi 10.1111/den.13465.
11. Tkach M, Thery C. Communication by Extracellular Vesicles: Where We Are and Where We Need to Go. Cell **2016**;164(6):1226-32 doi 10.1016/j.cell.2016.01.043.

12. Kahlert C, Kalluri R. Exosomes in tumor microenvironment influence cancer progression and metastasis. Journal of molecular medicine (Berlin, Germany) **2013**;91(4):431-7 doi 10.1007/s00109-013-1020-6.
13. Kosaka N, Iguchi H, Yoshioka Y, Takeshita F, Matsuki Y, Ochiya T. Secretory mechanisms and intercellular transfer of microRNAs in living cells. J Biol Chem **2010**;285(23):17442-52 doi 10.1074/jbc.M110.107821.
14. Hoshino A, Costa-Silva B, Shen TL, Rodrigues G, Hashimoto A, Tesic Mark M*, et al.* Tumour exosome integrins determine organotropic metastasis. Nature **2015**;527(7578):329-35 doi 10.1038/nature15756.
15. An T, Qin S, Xu Y, Tang Y, Huang Y, Situ B*, et al.* Exosomes serve as tumour markers for personalized diagnostics owing to their important role in cancer metastasis. Journal of Extracellular Vesicles **2015**;4(1):1-15 doi 10.3402/jev.v4.27522.
16. Jingushi K, Uemura M, Ohnishi N, Nakata W, Fujita K, Naito T*, et al.* Extracellular vesicles isolated from human renal cell carcinoma tissues disrupt vascular endothelial cell morphology via azurocidin. Int J Cancer **2018**;142(3):607-17 doi 10.1002/ijc.31080.
17. Okuda S, Watanabe Y, Moriya Y, Kawano S, Yamamoto T, Matsumoto M*, et al.* jPOSTrepo: an international standard data repository for proteomes. Nucleic Acids Res **2017**;45(D1):D1107-D11 doi 10.1093/nar/gkw1080.
18. Benjamini Y, Hochberg Y. Controlling the False Discovery Rate: A Practical and Powerful Approach to Multiple Testing. Journal of the Royal Statistical Society: Series B (Methodological) **1995**;57(1):289-300 doi 10.1111/j.2517-6161.1995.tb02031.x.
19. Lässer C, Eldh M, Lötvall J. Isolation and Characterization of RNA-Containing Exosomes. Journal of Visualized Experiments **2012**(59):1-6 doi 10.3791/3037.
20. Carpentier G, Martinelli M, Courty J, Cascone I. Angiogenesis Analyzer for ImageJ. 4th ImageJ User and Developer Conference proceedings, Mondorf-les-Bains, Luxembourg **2012**:198-201.
21. Saigusa D, Okamura Y, Motoike IN, Katoh Y, Kurosawa Y, Saijyo R*, et al.* Establishment of Protocols for Global Metabolomics by LC-MS for Biomarker Discovery. PLoS One **2016**;11(8):e0160555 doi 10.1371/journal.pone.0160555.
22. Hishinuma E, Narita Y, Saito S, Maekawa M, Akai F, Nakanishi Y*, et al.* Functional Characterization of 21 Allelic Variants of Dihydropyrimidine Dehydrogenase Identified in 1070 Japanese Individuals. Drug Metab Dispos **2018**;46(8):1083-90 doi 10.1124/dmd.118.081737.
23. Zhu B, Wei H, Wang Q, Li F, Dai J, Yan C*, et al.* A simultaneously quantitative method to profiling twenty endogenous nucleosides and nucleotides in cancer cells using

UHPLC-MS/MS. Talanta **2018**;179:615-23 doi 10.1016/j.talanta.2017.11.054.

24. Lu Y, Wang W, Wang J, Yang C, Mao H, Fu X*, et al.* Overexpression of arginine transporter CAT-1 is associated with accumulation of L-arginine and cell growth in human colorectal cancer tissue. PLoS One **2013**;8(9):e73866 doi 10.1371/journal.pone.0073866.
25. Fukumura D, Jain RK. Role of nitric oxide in angiogenesis and microcirculation in tumors. Cancer Metastasis Rev **1998**;17(1):77-89 doi 10.1023/a:1005908805527.
26. Gallo O, Masini E, Morbidelli L, Franchi A, Fini-Storchi I, Vergari WA*, et al.* Role of nitric oxide in angiogenesis and tumor progression in head and neck cancer. J Natl Cancer Inst **1998**;90(8):587-96 doi 10.1093/jnci/90.8.587.
27. Kim YH, Hwang JH, Kim KS, Noh JR, Gang GT, Seo Y*, et al.* NAD(P)H:quinone oxidoreductase 1 activation reduces blood pressure through regulation of endothelial nitric oxide synthase acetylation in spontaneously hypertensive rats. Am J Hypertens **2015**;28(1):50-7 doi 10.1093/ajh/hpu116.
28. Crabtree MJ, Hale AB, Channon KM. Dihydrofolate reductase protects endothelial nitric oxide synthase from uncoupling in tetrahydrobiopterin deficiency. Free Radic Biol Med **2011**;50(11):1639-46 doi 10.1016/j.freeradbiomed.2011.03.010.
29. Klatt P, Schmidt K, Werner ER, Mayer B. Determination of nitric oxide synthase cofactors: heme, FAD, FMN, and tetrahydrobiopterin. Methods Enzymol **1996**;268:358-65 doi 10.1016/s0076-6879(96)68038-0.
30. Gao L, Pung YF, Zhang J, Chen P, Wang T, Li M*, et al.* Sepiapterin reductase regulation of endothelial tetrahydrobiopterin and nitric oxide bioavailability. Am J Physiol Heart Circ Physiol **2009**;297(1):H331-9 doi 10.1152/ajpheart.00007.2009.
31. Abdelmagid SA, Rickard JA, McDonald WJ, Thomas LN, Too CK. CAT-1-mediated arginine uptake and regulation of nitric oxide synthases for the survival of human breast cancer cell lines. J Cell Biochem **2011**;112(4):1084-92 doi 10.1002/jcb.23022.
32. Hood J, Granger HJ. Protein kinase G mediates vascular endothelial growth factor-induced Raf-1 activation and proliferation in human endothelial cells. J Biol Chem **1998**;273(36):23504-8 doi 10.1074/jbc.273.36.23504.
33. Keerthikumar S, Chisanga D, Ariyaratne D, Al Saffar H, Anand S, Zhao K*, et al.* ExoCarta: A Web-Based Compendium of Exosomal Cargo. J Mol Biol **2016**;428(4):688-92 doi 10.1016/j.jmb.2015.09.019.
34. Jingushi K, Uemura M, Nakano K, Hayashi Y, Wang C, Ishizuya Y*, et al.* Leukocyteassociated immunoglobulinlike receptor 1 promotes tumorigenesis in RCC. Oncol Rep **2019**;41(2):1293-303 doi 10.3892/or.2018.6875.
35. Chen H, Chen XZ, Waterboer T, Castro FA, Brenner H. Viral infections and colorectal

cancer: a systematic review of epidemiological studies. Int J Cancer **2015**;137(1):12-24 doi 10.1002/ijc.29180.

36. Lane RE, Korbie D, Hill MM, Trau M. Extracellular vesicles as circulating cancer biomarkers: opportunities and challenges. Clin Transl Med **2018**;7(1):14 doi 10.1186/s40169-018-0192-7.
37. Chen Y, Tang Y, Fan GC, Duan DD. Extracellular vesicles as novel biomarkers and pharmaceutic targets of diseases. Acta Pharmacol Sin **2018**;39(4):499-500 doi 10.1038/aps.2018.15.
38. Rotmann A, Strand D, Martine U, Closs EI. Protein kinase C activation promotes the internalization of the human cationic amino acid transporter hCAT-1. A new regulatory mechanism for hCAT-1 activity. J Biol Chem **2004**;279(52):54185-92 doi 10.1074/jbc.M409556200.
39. Closs EI, Boissel JP, Habermeier A, Rotmann A. Structure and function of cationic amino acid transporters (CATs). The Journal of membrane biology **2006**;213(2):67-77 doi 10.1007/s00232-006-0875-7.
40. Hatzoglou M, Fernandez J, Yaman I, Closs E. Regulation of cationic amino acid transport: the story of the CAT-1 transporter. Annu Rev Nutr **2004**;24:377-99 doi 10.1146/annurev.nutr.23.011702.073120.
41. McDonald KK, Zharikov S, Block ER, Kilberg MS. A caveolar complex between the cationic amino acid transporter 1 and endothelial nitric-oxide synthase may explain the "arginine paradox". J Biol Chem **1997**;272(50):31213-6 doi 10.1074/jbc.272.50.31213.
42. Denninger JW, Marletta MA. Guanylate cyclase and the .NO/cGMP signaling pathway. Biochim Biophys Acta **1999**;1411(2-3):334-50 doi 10.1016/s0005-2728(99)00024-9.
43. Yoshizuka N, Chen RM, Xu Z, Liao R, Hong L, Hu WY*, et al.* A novel function of p38-regulated/activated kinase in endothelial cell migration and tumor angiogenesis. Mol Cell Biol **2012**;32(3):606-18 doi 10.1128/MCB.06301-11.
44. Rousseau S, Houle F, Landry J, Huot J. p38 MAP kinase activation by vascular endothelial growth factor mediates actin reorganization and cell migration in human endothelial cells. Oncogene **1997**;15(18):2169-77 doi 10.1038/sj.onc.1201380.

Acknowledgements

This study was supported by the grant from Project for Cancer Research and Therapeutic Evolution in Japan Agency for Medical Research and Development (AMED).

Author contributions

Conception, design and study supervision: K. Ueda

Acquisition of data: A. Ikeda, M. Sumazaki, M. Konishi, R. Fujii, S. Muraoka, D. Saigusa

Analysis and interpretation of data (e.g., statistical analysis, biostatistics, computational analysis): A. Ikeda, N. Saichi

Writing of the manuscript: A. Ikeda

Collecting clinical samples: S. Nagayama

Others (scientific discussions): Y. Sakai, H. Shimada

Data availability

All the LC/MS raw data was deposited in Japan Proteome Standard Repository/Database (JPOST, ID: JPST000867). Further data are available from the corresponding authors upon reasonable request.

Materials & Correspondence

Correspondence and requests for materials should be addressed to K.U.

Figure Legends

Fig. 1 Extraction of tissue-exudative extracellular vesicles (Te-EVs) from colorectal cancer (CRC) tissues. (**a**) Schematic illustration for preparation and proteomic analysis of tissue exudative extracellular vesicles (Te-EVs) is shown. Te-EVs were isolated from freshly resected primary colorectal cancer (CRC) tissues or adjacent normal mucosa (n = 17). Comprehensive proteome analysis was performed with LC/MS for Te-EVs and also original tissues. (**b**) Evaluation of molecular characteristics of Te-EVs by western blotting of EV marker proteins, CD63 and CD81. 10 μg of protein was loaded to each lane. (**c**) Relative protein abundances of CD63 or CD81 in (**b**) were shown in the bar charts. N: adjacent normal mucosa, T: primary colorectal cancer.

Fig. 2 Proteomic overview of CRC Te-EVs and tissues. (**a**) The Venn diagram shows number of identified proteins in CRC tissues or Te-EVs by LC/MS analysis. (**b**) Quantitative relationship was assessed between tissue proteome and Te-EV proteome. The plots shows proteins that were commonly identified both in Te-EVs and tissues by LC/MS analysis. The X and Y axis represent averaged relative protein abundances. The right panel shows the magnified view around the origin. Coefficient of determination (R^2) is shown. (**c**) Representative EV marker proteins, CD9, CD63, and CD151 were highly enriched in Te-EVs compared to tissues. (**d**) A newly identified class of EV luminal markers, vacuolar protein sorting (VPS) family proteins, also demonstrated significantly higher expressions in Te-EVs than those in tissues. (**e**) The Venn diagram shows comparison between the deposited proteins in the ExoCarta database and the identified total Te-EV proteins in this study. (**f**) The Venn diagram shows comparison between the deposited proteins as CRC EV proteins in the ExoCarta database and the identified proteins from tumor region-derived Te-EVs in this study.

Fig. 3 Identification of CAT1 as a specific surface antigen on CEC-derived EVs. (**a**) The result of differential analysis based on paired t-test between proteome from tumor region-derived EVs (tumor Te-EVs) and that from normal mucosa-derived EVs (normal Te-EVs) is displayed as the volcano plot. Significantly up-regulated 487 proteins (adjusted $p < 0.05$ and fold-change > 5.0) or down-regulated 88 proteins (adjusted $p < 0.05$ and fold-change < 0.2) were indicated in red or blue dots. (**b**) Principal component analysis was performed for top 100 up-regulated proteins in (**a**). (**c**) The line chart shows LC/MS-based relative protein abundances of CAT1 on EVs in 17 paired samples. (**d**) A representative image of transmission electron microscopy (TEM) for tumor Te-EVs. The black dot on the surface of the EV indicates the signal of the gold particle-labeled anti-CAT1 antibody. Bar: 200 nm. The expression of CAT1 was positive in 24 out of 74 (32,4%) of tumor Te-EVs while none (0/66) of normal Te-EVs were CAT1 positive. (**e**) Expression of CAT1 and CD9 in normal (N) and tumor (T) Te-EVs were confirmed by western blotting. (**f**) The CD9-normalized protein abundances of CAT1 in (**e**) were displayed with the box plot. (**g**) Representative images of immunohistochemical (IHC) staining of CAT1 in CRC tissues. The expression levels of CAT1 was classified into 3 groups as indicated. Bars: 50 μm. (**h**) The result of IHC staining of CAT1 for 75 samples was summarized with the violin plot. N: normal colon mucosa tissue, I-IV: tissues of pathological stage I-IV CRC.

Fig. 4 The diagnostic potential of plasma EV-CAT1 for detection of CRC. (**a**) The framework of anti-CAT1 and anti-CD81 EV-sandwich ELISA is shown. B: biotin, SA: streptavidin, HRP: horseradish peroxidase, TMB: 3,3',5,5'-tetramethylbenzidine. (**b**) The result of EV-CAT1 sandwich ELISA measuring 119

plasma samples is displayed as the box plot. N: normal donors, I-IV: plasma from pathological stage I-IV CRC patients. The *p*-values were calculated by Student's *t*-test. (**c**) The diagnostic potential to distinguish CRC patients (n = 94) from normal donors (n = 25) was assessed by ROC curve analysis. In addition to the single usage of EV-CAT1 or CEA, the combination biomarker model, EV-CAT1 + CEA, was also evaluated based on logistic regression. AUC: area under the curve.

Fig.5 CAT1-dependent promotion of cell growth and tubule formation of HUBEC via EVs. (**a**) Representative images of IHC staining for CAT1 (A, C, E, G, I, K) or CD31 (B, D, F, H, J, L) are shown. CD31 (PECAM1) was stained as a marker for vascular endothelial cells. Serial sections were used for the comparison between the IHC staining of CAT1 and CD31. (**b**) The rate of moderate to strong-CAT1 expression in vascular endothelial cells of or near CRC tissues was significantly higher than that of adjacent normal tissues. (**c**) The high expression of CAT1 in HCT116 cells transfected with pCAGGS-CAT1-FLAG (CAT1-overexpressing HCT116) compared with those transfected with pCAGGS-FLAG (Control HCT116) was observed. (d) The expression level of CAT1 or CD9 was examined for EVs purified from CAT1-overexpressed HCT116 cells ($CAT1^{++}$-EVs) or mock-transfected cells (mock-EVs). (**e**) A representative image of TEM for mock-EV or $CAT1^{++}$-EV is shown. The black dot on the surface of the EV indicates the signal of the gold particle-labeled anti-CAT1 antibody. Bar: 50 nm. (**f**) Fluorescent microscopic images of HUVEC 4 hours after treatment with PBS or fluorescence-labeled $CAT1^{++}$-EV. Bar: 5 μm. (**g**) Fluorescent microscopic images of HUVEC 72 hours after treatment with PBS or $CAT1^{++}$-EV. The expression of CAT1 was detected by the Alexa 488-labeled secondary antibody. Bar: 5 μm. (**h, i**) The expression of CAT1 (**h**) or the growth activity (**i**) was measured in HUVEC 72 hours after treatment with PBS, mock-EV, or $CAT1^{++}$-EV.

Each error bars are presented as the mean SE (n = 3). (**j**) Representative images of tube formation assay. 72 hours after treatment with PBS, mock-EV, or CAT1^{++}-EV, HUVEC was cultured in matrigel plates for 24 hours. (**k**) The relative total tube length in (j) was measured by Image-J. Each error bar is presented as the mean SE (n = 3).

Fig.6 CAT1-dependent modulation of NO metabolic pathway in vascular endothelial cells. (**a**) Expression level of CAT1 was measured in mock-transfected HUVEC (HUVEC-mock) or CAT1-overexpressed HUVEC (HUVEC-CAT1). (**b**) The results of quantitative metabolomic analysis for the arginine/NO/cGMP pathway was illustrated. Absolute quantification of the metabolites was performed for HUVEC-mock or HUVEC-CAT1 after stimulation with arginine for 15 min. Each error bar is presented as the mean SE (n = 4). (**c**) Cyclic GMP concentrations of HUVEC treated with CAT1^{++}-EVs or mock-EVs were compared. Each error bars are presented as the mean SE (n = 3). (d) An illustration of CAT1 transfer from CRC cells to vascular endothelial cells via EVs in tumor microenvironment. Putative signaling pathway in a vascular endothelial cell from the arginine/NO/cGMP pathway to its downstream is shown. Arg: arginine, eNOS: endothelial nitric oxide synthase, NADPH: nicotinamide adenine dinucleotide phosphate, NADP: nicotinamide adenine dinucleotide phosphate, NHA: N$^{\omega}$-hydroxy-L-arginine, NO: nitric oxide, Cit: citrulline, sGC: soluble guanylate cyclase, GTP: guanosine triphosphate, cGMP: cyclic guanosine monophosphate, PRAK: p38-regulated/activated kinase, FAK: Focal adhesion kinase.

Figure. 1

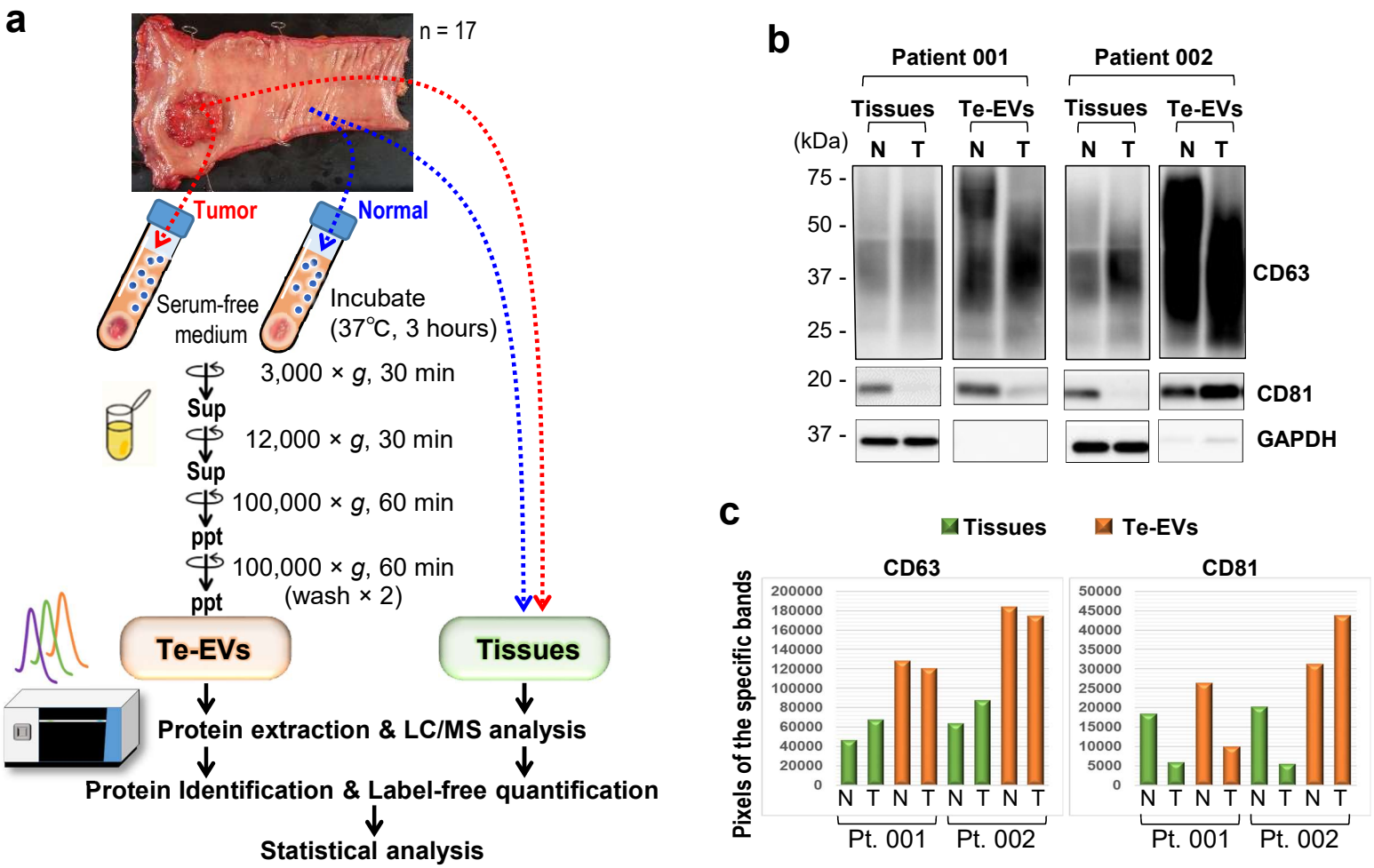
a
n = 17
Tumor
Normal
Serum-free medium
Incubate (37℃, 3 hours)
3,000 × g, 30 min
Sup
12,000 × g, 30 min
Sup
100,000 × g, 60 min
ppt
100,000 × g, 60 min (wash × 2)
ppt
Te-EVs
Tissues
Protein extraction & LC/MS analysis
Protein Identification & Label-free quantification
Statistical analysis
b
Patient 001
Patient 002
Tissues
Te-EVs
Tissues
Te-EVs
(kDa)
N T N T N T N T
75 -
50 -
37 -
25 -
20 -
37 -
CD63
CD81
GAPDH
c
Tissues
Te-EVs
CD63
CD81
Pixels of the specific bands
200000
180000
160000
140000
120000
100000
80000
60000
40000
20000
0
50000
45000
40000
35000
30000
25000
20000
15000
10000
5000
0
N T N T N T N T
Pt. 001
Pt. 002
Pt. 001
Pt. 002

Figure. 2

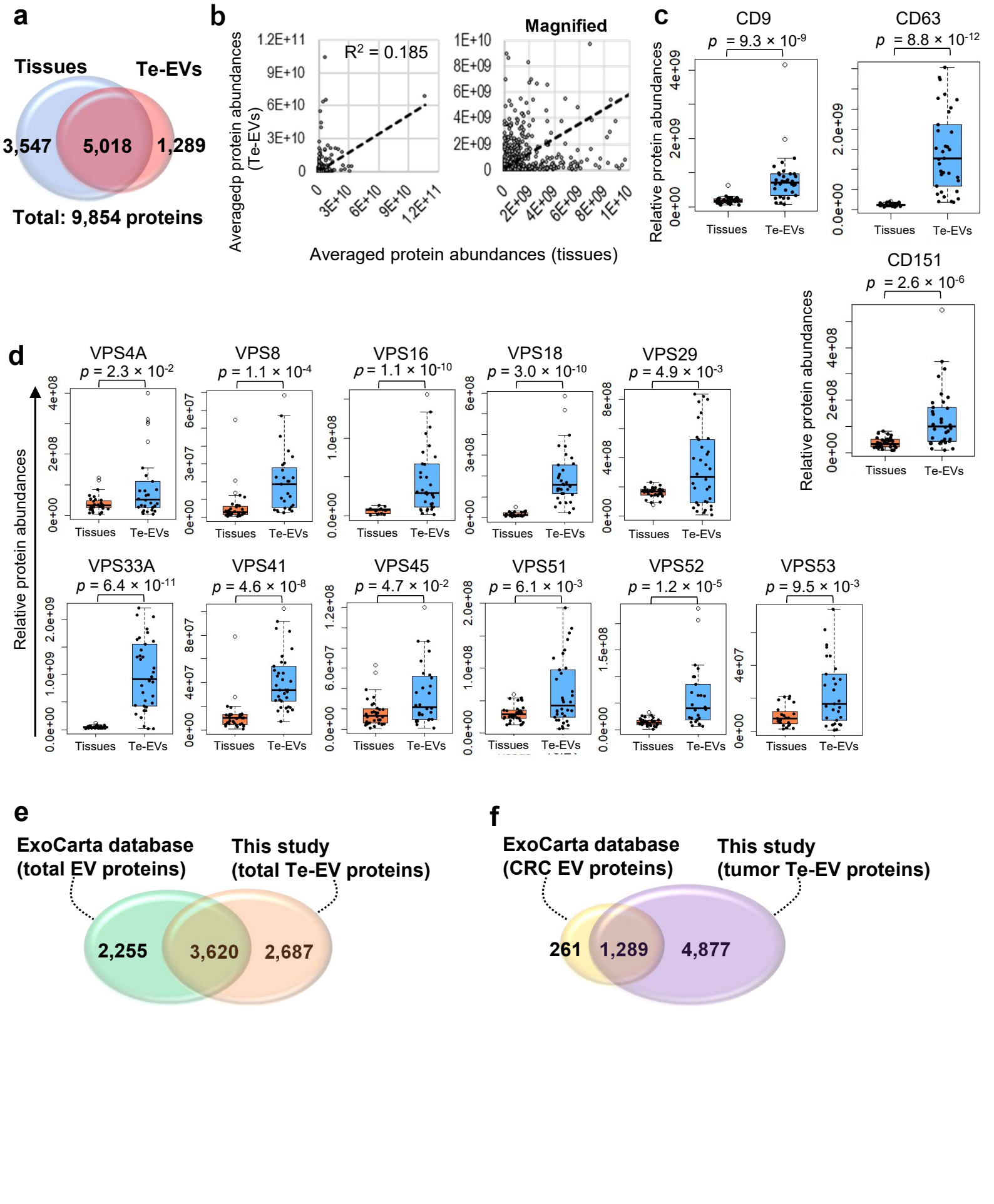
a
Tissues
Te-EVs
3,547
5,018
1,289
Total: 9,854 proteins
b
R² = 0.185
Magnified
Averagedp protein abundances (Te-EVs)
Averaged protein abundances (tissues)
c
CD9
p = 9.3 × 10-9
CD63
p = 8.8 × 10-12
CD151
p = 2.6 × 10-6
Relative protein abundances
Tissues
Te-EVs
d
VPS4A
p = 2.3 × 10-2
VPS8
p = 1.1 × 10-4
VPS16
p = 1.1 × 10-10
VPS18
p = 3.0 × 10-10
VPS29
p = 4.9 × 10-3
VPS33A
p = 6.4 × 10-11
VPS41
p = 4.6 × 10-8
VPS45
p = 4.7 × 10-2
VPS51
p = 6.1 × 10-3
VPS52
p = 1.2 × 10-5
VPS53
p = 9.5 × 10-3
Relative protein abundances
e
ExoCarta database (total EV proteins)
This study (total Te-EV proteins)
2,255
3,620
2,687
f
ExoCarta database (CRC EV proteins)
This study (tumor Te-EV proteins)
261
1,289
4,877

Figure. 3

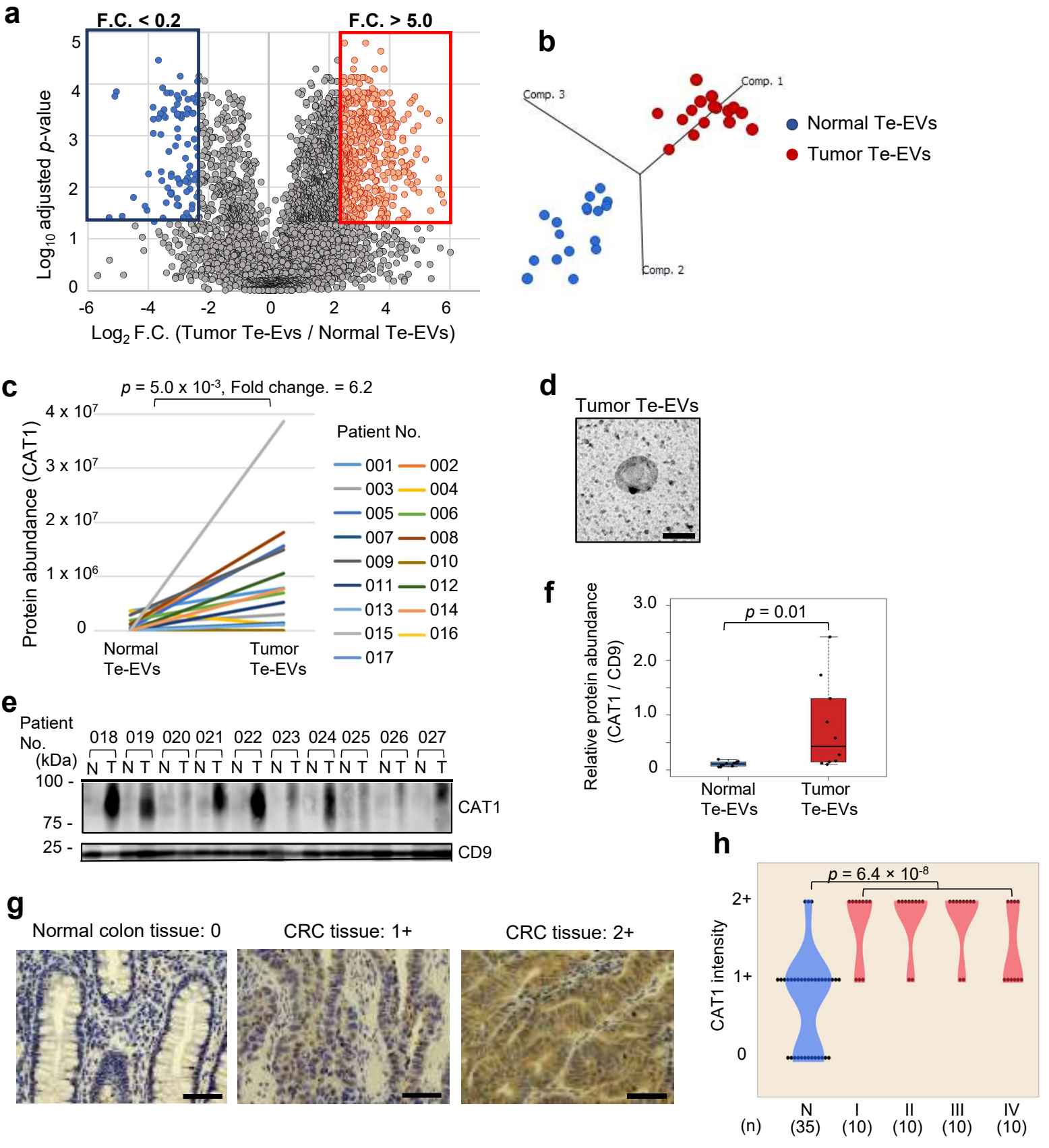
a
F.C. < 0.2
F.C. > 5.0
Log10 adjusted p-value
Log2 F.C. (Tumor Te-Evs / Normal Te-EVs)
b
Comp. 1
Comp. 3
Comp. 2
Normal Te-EVs
Tumor Te-EVs
c
p = 5.0 x 10-3, Fold change. = 6.2
Protein abundance (CAT1)
Patient No.
001 002 003 004 005 006 007 008 009 010 011 012 013 014 015 016 017
Normal Te-EVs
Tumor Te-EVs
d
Tumor Te-EVs
e
Patient No.
018 019 020 021 022 023 024 025 026 027
N T N T N T N T N T N T N T N T N T
(kDa)
100 -
75 -
25 -
CAT1
CD9
f
p = 0.01
Relative protein abundance (CAT1 / CD9)
Normal Te-EVs
Tumor Te-EVs
g
Normal colon tissue: 0
CRC tissue: 1+
CRC tissue: 2+
h
p = 6.4 × 10-8
CAT1 intensity
(n)
N (35)
I (10)
II (10)
III (10)
IV (10)

Figure. 4

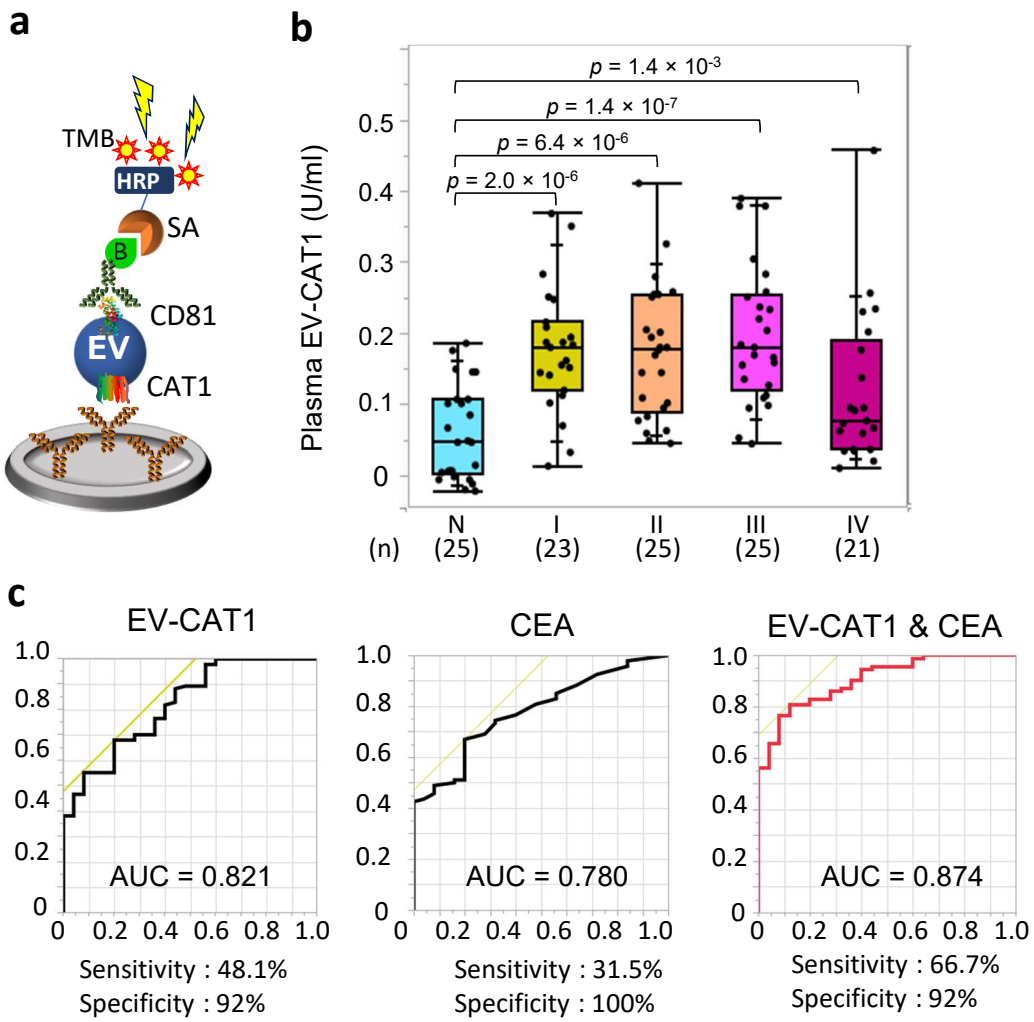
a
TMB
HRP
SA
B
CD81
EV
CAT1
b
p = 1.4 × 10-3
p = 1.4 × 10-7
p = 6.4 × 10-6
p = 2.0 × 10-6
Plasma EV-CAT1 (U/ml)
0.5
0.4
0.3
0.2
0.1
0
(n)
N (25)
I (23)
II (25)
III (25)
IV (21)
c
EV-CAT1
AUC = 0.821
Sensitivity : 48.1%
Specificity : 92%
CEA
AUC = 0.780
Sensitivity : 31.5%
Specificity : 100%
EV-CAT1 & CEA
AUC = 0.874
Sensitivity : 66.7%
Specificity : 92%

Figure. 5

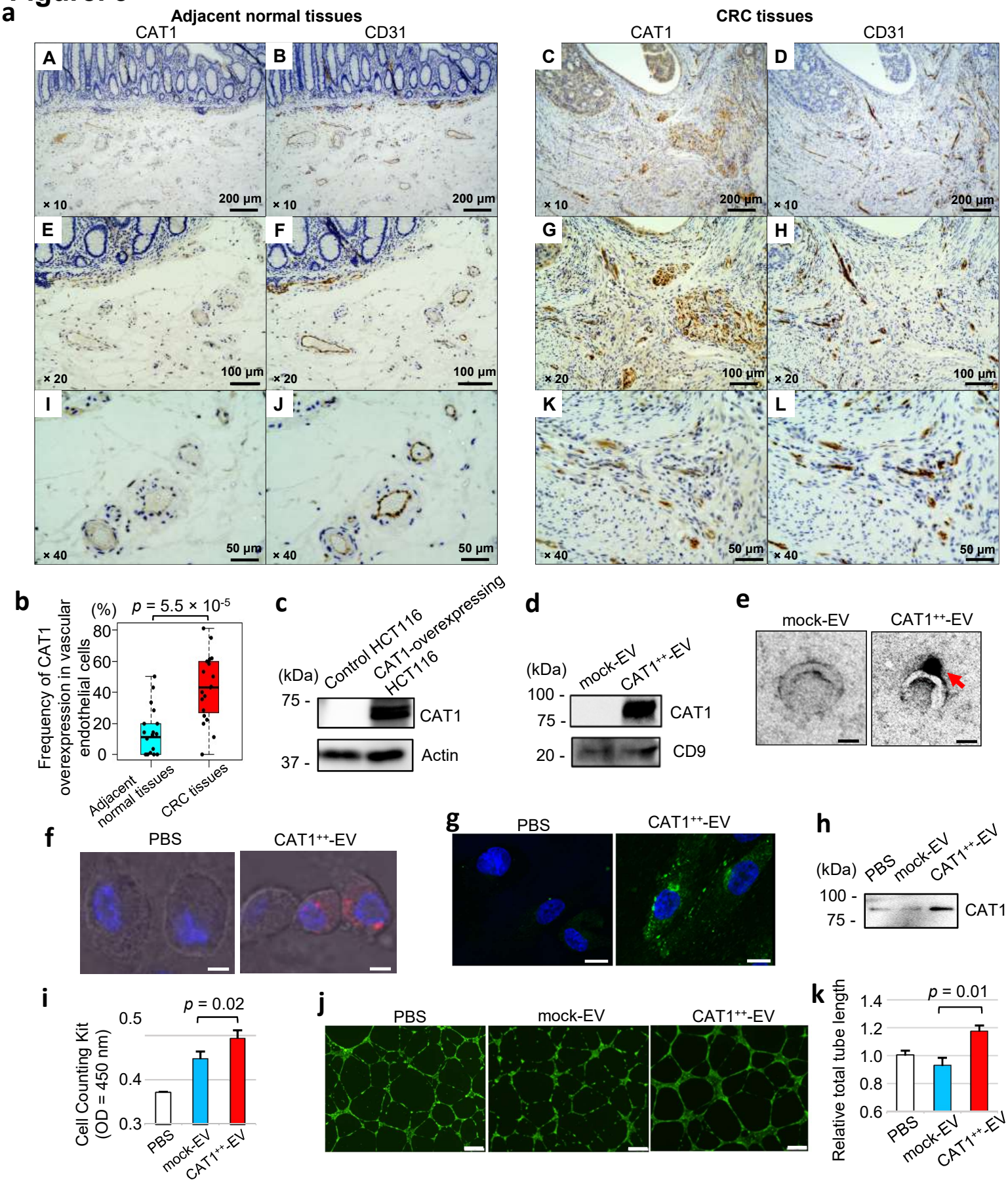
a
Adjacent normal tissues
CRC tissues
CAT1
CD31
A
B
C
D
E
F
G
H
I
J
K
L
× 10
× 20
× 40
200 μm
100 μm
50 μm
b
Frequency of CAT1 overexpression in vascular endothelial cells
(%)
p = 5.5 × 10-5
Adjacent normal tissues
CRC tissues
c
(kDa)
Control HCT116
CAT1-overexpressing HCT116
75 -
37 -
CAT1
Actin
d
(kDa)
mock-EV
CAT1++-EV
100 -
75 -
20 -
CAT1
CD9
e
mock-EV
CAT1++-EV
f
PBS
CAT1++-EV
g
PBS
CAT1++-EV
h
(kDa)
PBS
mock-EV
CAT1++-EV
100 -
75 -
CAT1
i
Cell Counting Kit (OD = 450 nm)
p = 0.02
0.5
0.4
0.3
PBS
mock-EV
CAT1++-EV
j
PBS
mock-EV
CAT1++-EV
k
Relative total tube length
p = 0.01
1.4
1.2
1.0
0.8
0.6
PBS
mock-EV
CAT1++-EV

Figure. 6

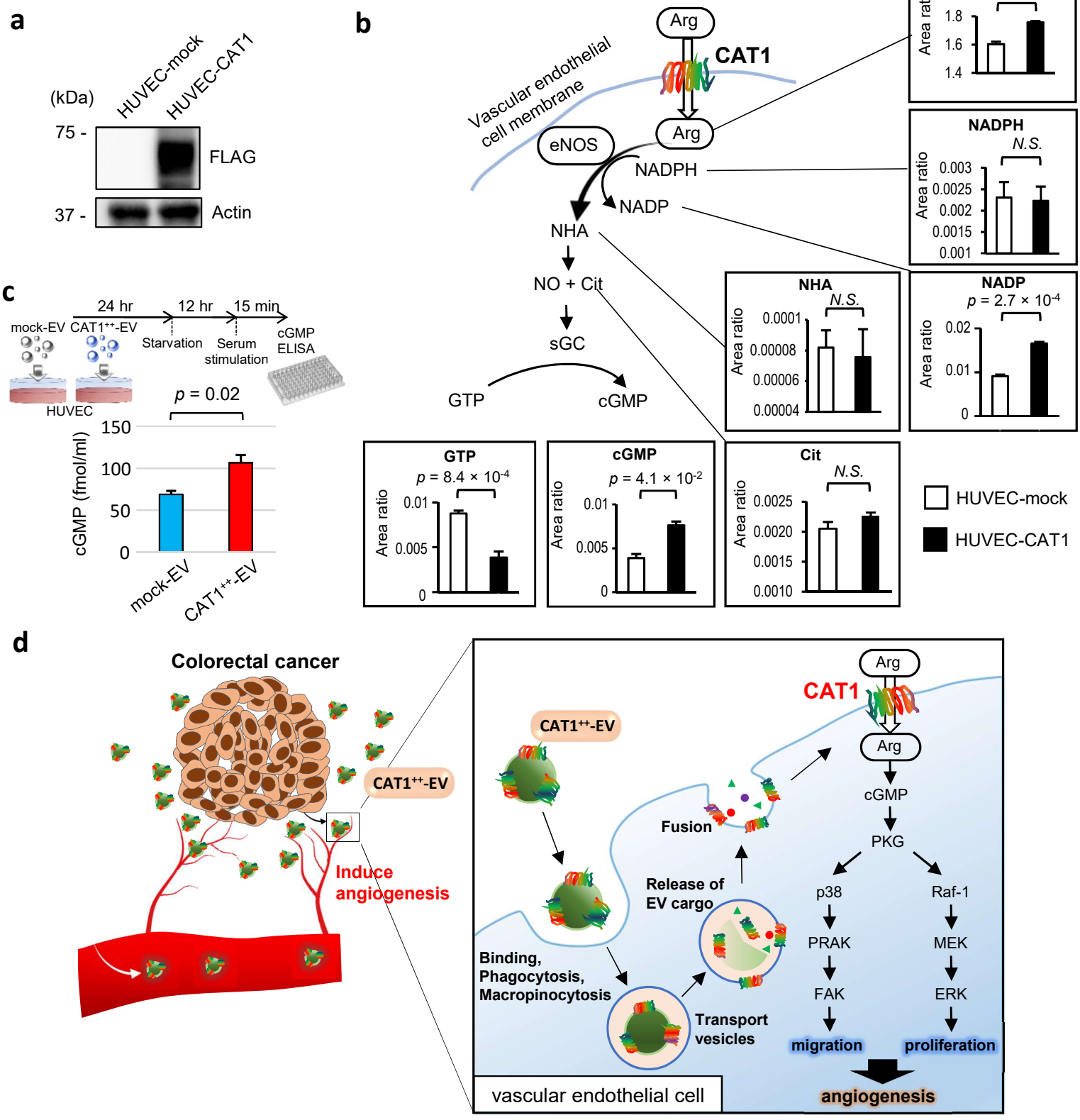
a
(kDa)
HUVEC-mock
HUVEC-CAT1
75 -
FLAG
37 -
Actin
b
Vascular endothelial cell membrane
Arg
CAT1
Arg
eNOS
NADPH
NADP
NHA
NO + Cit
sGC
GTP
cGMP
Arg
p = 2.8× 10-2
Area ratio
NADPH
N.S.
NADP
p = 2.7 × 10-4
NHA
N.S.
GTP
p = 8.4 × 10-4
cGMP
p = 4.1 × 10-2
Cit
N.S.
HUVEC-mock
HUVEC-CAT1
c
24 hr
12 hr
15 min
mock-EV
CAT1++-EV
Starvation
Serum stimulation
cGMP ELISA
HUVEC
p = 0.02
cGMP (fmol/ml)
mock-EV
CAT1++-EV
d
Colorectal cancer
CAT1++-EV
Induce angiogenesis
CAT1++-EV
Arg
CAT1
Arg
cGMP
PKG
Fusion
Release of EV cargo
Binding, Phagocytosis, Macropinocytosis
Transport vesicles
p38
PRAK
FAK
migration
Raf-1
MEK
ERK
proliferation
angiogenesis
vascular endothelial cell

Supplementary information summary

- **Supplementary figure 1**
  Quantitative distribution of CRC Te-EV proteome
- **Supplementary figure 2**
  Gene ontology (GO)-based functional assessment of CRC-derived Te-EVs
- **Supplementary figure 3**
  Quantitative correlation between plasma EV-CAT1 and CEA
- **Supplementary figure 4**
  Proteomic difference between Te-EVs and original tissues
- **Supplementary figure 5**
  The distribution of subcellular localization for Te-EV or original tissue proteins

- **Supplementary table 1**
  Clinical information and protein abundances in LC/MS analysis
  of the CRC patients and the healthy donors.
- **Supplementary table 2**
  The list of identified 8,565 CRC tissue proteins.
- **Supplementary table 3**
  The list of identified 6,307 CRC Te-EV proteins.
- **Supplementary table 4**
  The 487 EV biomarker candidates for CRC (adjusted $p < 0.05$ and fold-change > 5.0, paired t-test).
- **Supplementary table 5**
  The focused 11 EV biomarker candidates for CRC selected as surface antigens for
  EV-sandwich ELISA (adjusted $p < 0.05$ and fold-change > 5.0, paired t-test).
- **Supplementary table 6**
  Results of gene ontology analyses for up-regulated proteins in CRC tumor Te-EVs.
- **Supplementary table 7**
  Top 100 of up-regulated and down-regulated Te-EV proteins compared with tissue proteins.
- **Supplementary table 8**
  Enriched KEGG pathways (up-regulated 487 proteins in tumor Te-EVs)..

Supplementary figure. 1

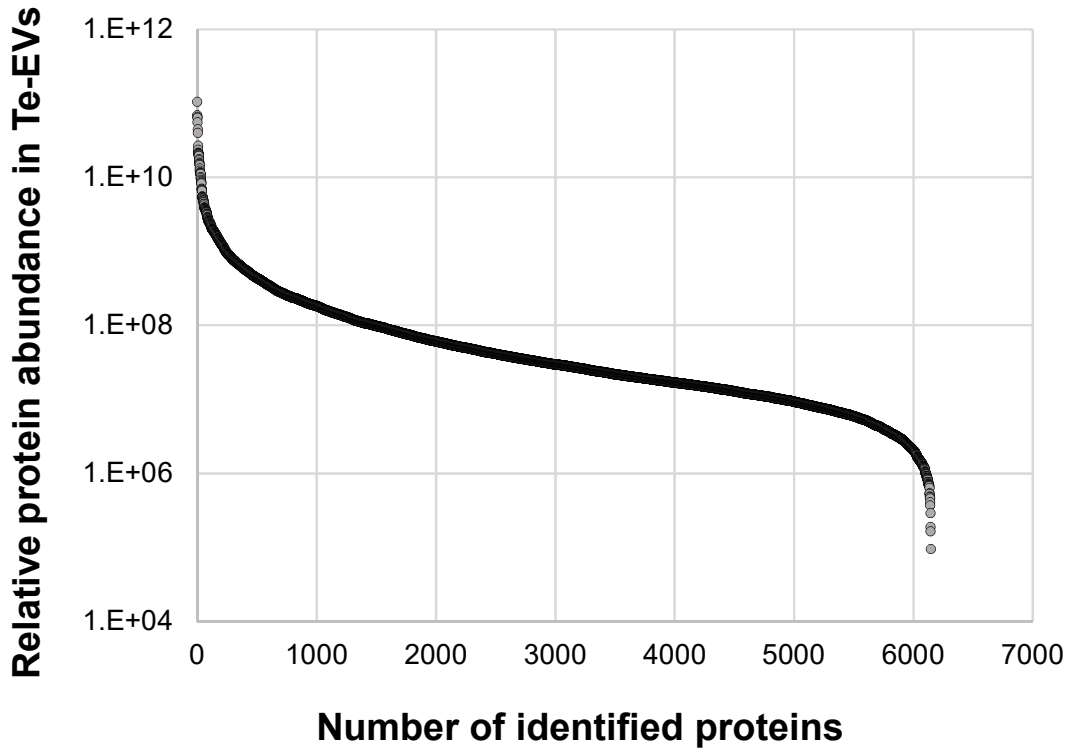

Supplementary figure 1

Dynamic range plot of quantified Te-EV proteome. The X axis indicates abundance rank of qualified Te-EV proteome, and the Y axis indicates the relative abundance by the LC/MS analysis.

Supplementary figure. 2

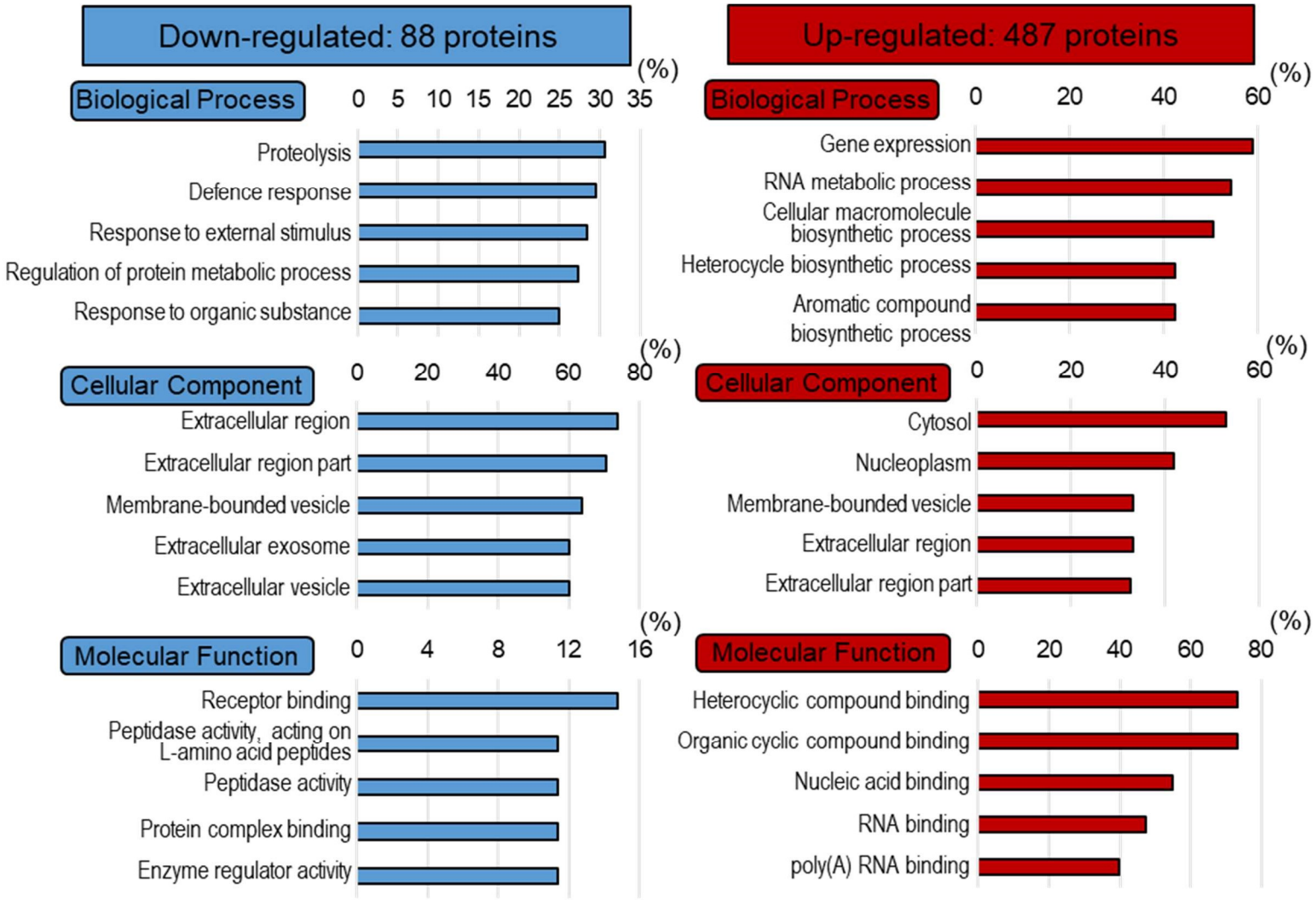

Supplementary figure 2

GO analysis of up-regulated (fold change > 5, adjusted $p < 0.05$) and down-regulated (fold change < 0.02, adjusted $p < 0.05$) proteins in tumor Te-EVs._For biological process, cellular component and molecular function, data of GOTERM_BP_FAT, GOTERM_CC_FAT and GOTERM_MF_FAT were used from Gene_Ontology in Functional Annotation Tool on the website, respectively. The Y axis indicates the percentage of the annotated proteins.

Supplementary figure. 3

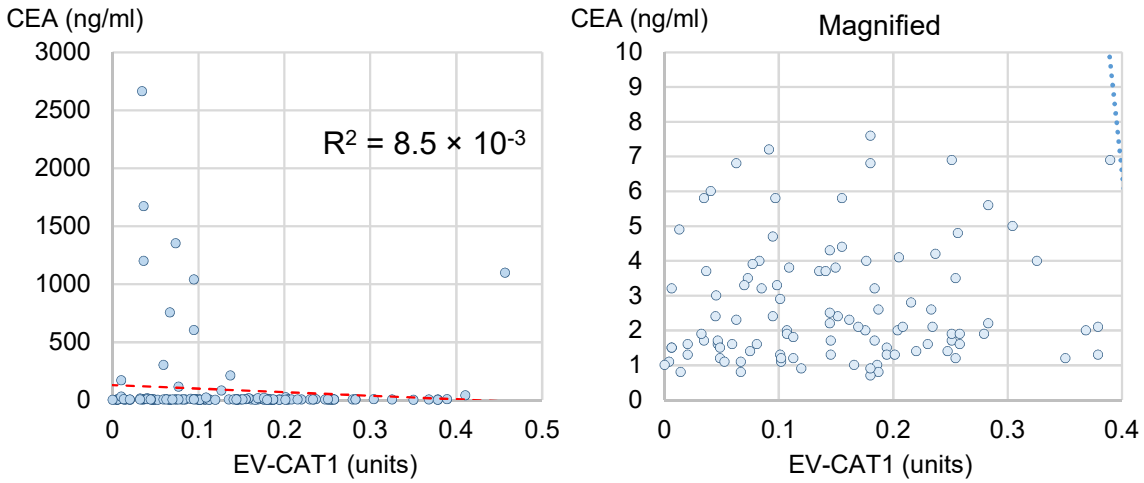

Supplementary figure 3

Scatter plot showing EV-CAT1 sandwich ELISA (unit) on the X axis and preoperative CEA (ng / ml) on the Y axis (left). Magnified view of the plot is also shown (right). Coefficient of correlation value was 8.5×10^{-3}.

Supplementary Figure. 4

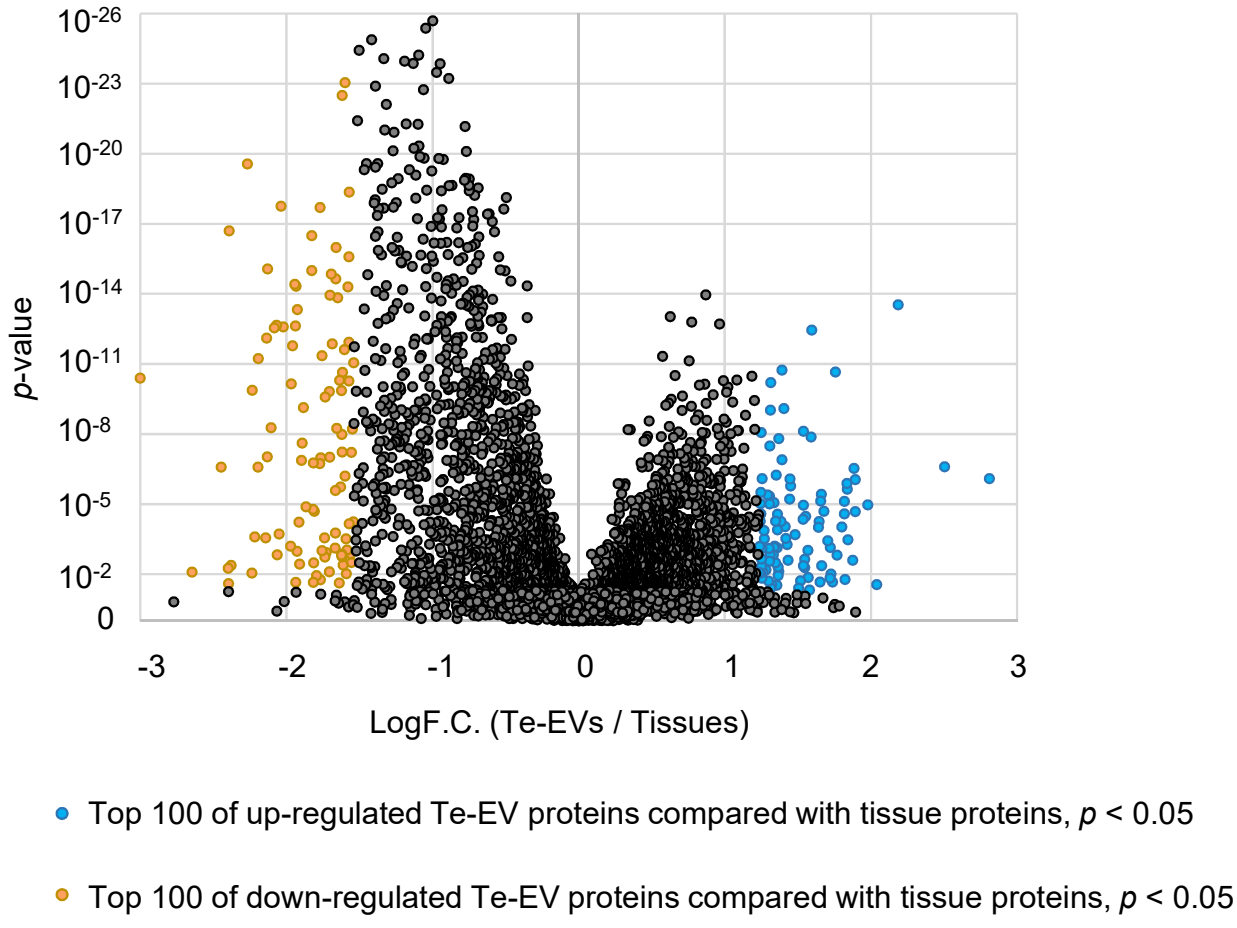

Supplementary figure 4

Volcano plot indicating *p*-value (Te-EVs vs. tissues) on the Y axis and log ratio (Te-EVs / tissue) of LC/MS intensity on the X axis. Blue dots indicate the top 100 Te-EV proteins which are significantly up-regulated than tissue proteins, and orange dots indicate the top 100 proteins which are significantly down-regulated than tissue proteins.

Supplementary figure. 5

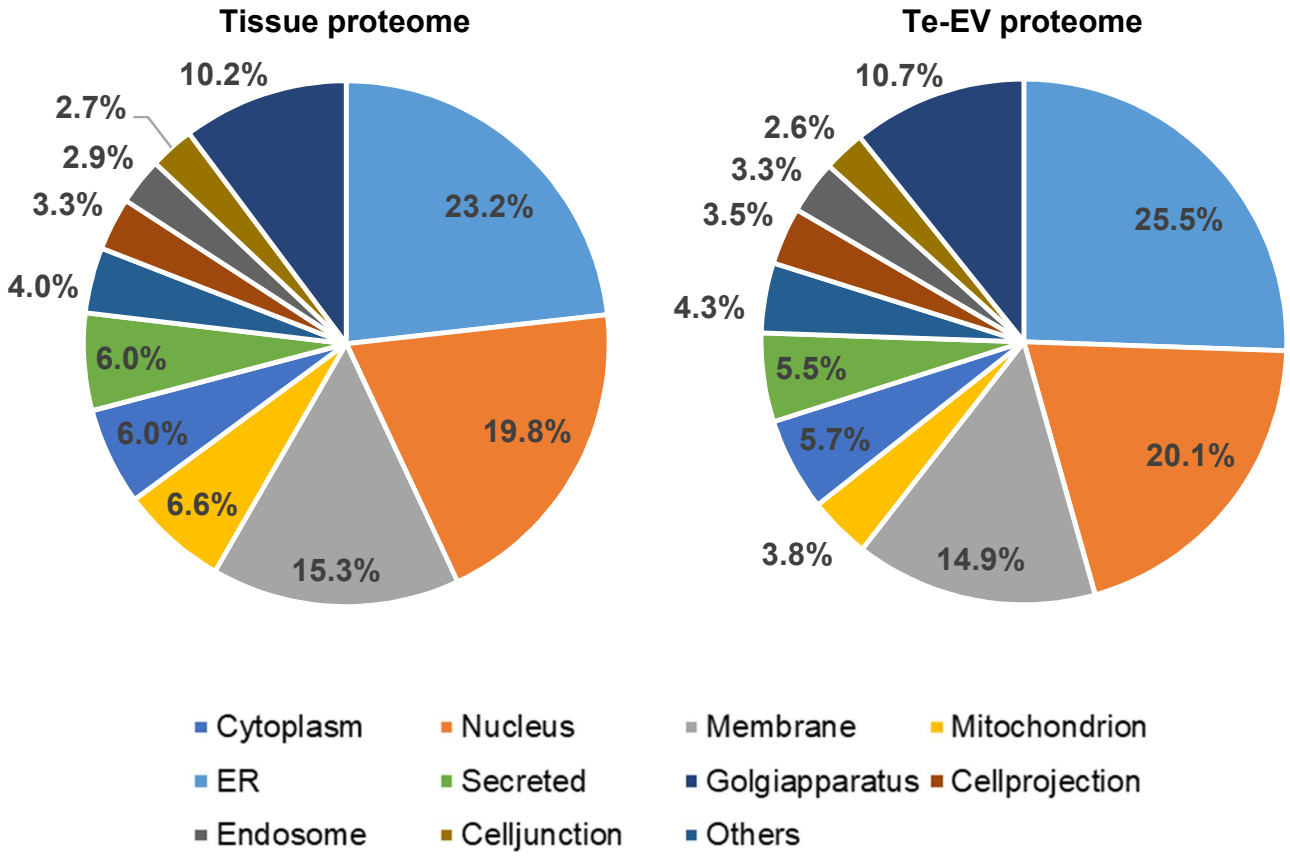

Supplementary figure 5

The analyses of subcellular proteome localisations are shown. The subcellular locations of tissues and Te-EVs are obtained on the Uniprot website. The distribution of the two proteome is similar with each other. The numbers show percentages.

Supplementary tables can be downloaded at

https://mcr.aacrjournals.org/content/suppl/2021/02/11/1541-7786.MCR-20-0827.DC1